

## ELECTRONIC SUPPORTING INFORMATION

### Anion-tunable control of the thermal $Z \rightarrow E$ isomerisation of the basic azobenzene receptors

Kajetan Dąbrowa,<sup>a</sup> Patryk Niedbała<sup>a</sup> and Janusz Jurczak<sup>\*,a</sup>

<sup>a</sup> Institute of Organic Chemistry, Polish Academy of Sciences,  
Kasprzaka 44/52, 01-224 Warsaw, Poland.  
E-mail: janusz.jurczak@icho.edu.pl

#### Contents

<b>1. SYNTHETIC PROCEDURES AND STRUCTURAL ANALYSIS</b>	<b>2</b>
1.1 General Remarks	2
1.2 Photoisomerisation	2
1.3 Synthetic pathway and substance analysis	2
1.4 Copies of <sup>1</sup> H and <sup>13</sup> C NMR spectra	4
<b>2. BINDING STUDIES</b>	<b>9</b>
2.1 General remarks	9
2.2 <sup>1</sup> H NMR titration experiments	9
2.3 <sup>1</sup> H NMR Job plot experiments	14
2.4 DFT Calculations	14
2.5 Visualization of the DFT calculated structures	16
2.6 Determination of the first-order rate constant $k_{\text{obs}}$ using UV-Vis spectroscopy	27
2.7 Procedure for the determination of association constant $K_{a,Z}$ and first-order rate constant $k_2$ from “ $Z \rightarrow E$ thermal titration” experiment	28
2.8 Cartesian coordinates of calculated DFT structures	30
<b>REFERENCES</b>	<b>34</b>

# 1. Synthetic Procedures and Structural Analysis

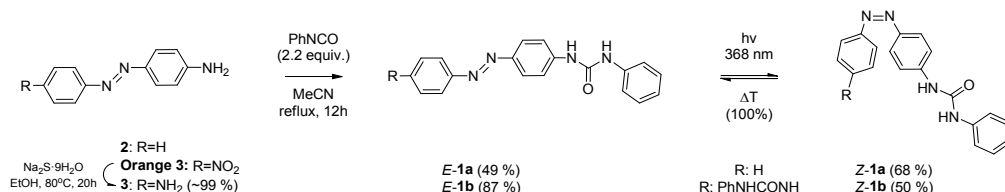
## 1.1 General Remarks

All solvents were of reagent grade quality. All reagents were purchased from Sigma-Aldrich and TCI Chemicals and used without further purification. Column chromatography was carried out using Merck Kieselgel 60 (63–100  $\mu\text{m}$  mesh size), TLC was carried out on Merck Kieselgel F254 plates. Melting points were determined using a Boëtius M HMK hot-stage apparatus and were uncorrected. The NMR spectra were recorded on a Varian Gemini 2000, Mercury 400, or Varian S600 instruments. Chemical shifts are reported in ppm and are set to solvent residue peak. The splitting pattern of multiplets is described by abbreviations (s – singlet, d – doublet, t – triplet, q – quartet, dd – doublet of doublets, m – multiplet, c – covered signal, b – broad peak).  $J$  coupling constants values are reported in Hz. Mass spectral analyses were performed with the ESI-TOF technique on a Mariner mass spectrometer from PerSeptive Biosystem. The UV-Vis spectra were recorded using Agilent Technologies Cary 60 spectrophotometer equipped with a Peltier thermostated cell holder (temperature accuracy  $\pm 0.1$  °C).

## 1.2 Photoisomerisation

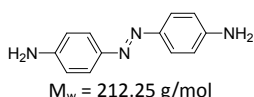
UV irradiation experiments were carried with a self-constructed Rayonet type photoreactor, equipped with eight UVA lamps (GE® F9BX BL G23 9W,  $\lambda_{\text{max}} = 368$  nm) and with an effective air cooling system to maintain fixed temperature ( $\leq 26$ °C) inside photoreactor chamber. To ensure homogenous irradiation, sample was spinned at 4 rpm. Photoisomerisation of the studied compounds was carried out in quartz cuvette (Hellma Analytics Quartz Suprasil 100-QS V = 3.5 ml, l = 10 mm) or in quartz NMR tube (Wilmad 535-PP-7QTZ,  $\phi = 5$  mm, limit 600 MHz). Time required to reach photostationary state (PSS) was found to be *ca.* 30 s for diluted receptor solution ( $c \sim 10^{-5}$  M) and 10-30 min for concentrated receptor solution ( $c \sim 10^{-2}$  M). Blue light irradiation experiments were carried out with SMD Power-LED bulb (3.3 W,  $\lambda_{\text{max}} = 410$  nm). UVA light intensity inside photoreactor chamber was measured by ferrioxalate actinometry<sup>1</sup> to be  $2.3 \pm 0.1 \cdot 10^{20}$  (quanta/L·s).

## 1.3 Synthetic pathway and substance analysis



Scheme S1. Synthesis of receptors **1a** and **1b**

### Compound **3**



<sup>1</sup>H NMR (400 MHz, DMSO)

<sup>13</sup>C NMR (100 MHz, DMSO)

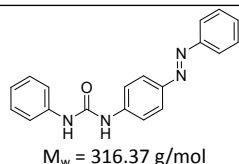
A solution of Disperse Orange 3 (10.0 g, 37 mmol, 90% purity) and sodium sulfide nonahydrate (19.50 g, 74 mmol, 2 equiv) in ethanol (600 ml) was refluxed for 20h. The solvent was evaporated under vacuum and resulting brown oil was redissolved in a mixture of water (500 ml) and brine (30 ml), extracted with ethyl acetate (3 x 300 ml), dried (MgSO<sub>4</sub>), concentrated (~100 ml), and passed through short pad of silica gel (~50 g) to afford **3** (7.82 g, ~99%) as a reddish solid (mp. 244°C, lit. 238-241).

$R_{f,3} = 0.55$ ,  $R_{f,2}$  (Disperse Orange 3) = 0.74 (hexanes - ethyl acetate 1:1 v/v)

$\delta$  7.55 (d,  $J = 8.8$  Hz, 4H), 6.65 (d,  $J = 8.8$  Hz, 4H), 5.73 (s, 4H).

$\delta$  151.0, 143.2, 123.9, 113.6.

### Host **E-1a**



<sup>1</sup>H NMR (200 MHz, DMSO)

<sup>13</sup>C NMR (50 MHz, DMSO)

HRMS ESI (m/z)

Anal (%)

The mixture of 4-aminoazobenzene **3** (1.0 g, 5.1 mmol) and phenyl isocyanate (0.60 mL, 5.6 mmol, 1.1 equiv) was refluxed in anhydrous acetonitrile (20 mL) overnight under argon atmosphere. Then the orange product was filtered off, washed with cold acetonitrile (10 mL) and diethyl ether (20 mL), and dried at high vacuum to give host **E-1a** (0.72 g, 44 %) as yellowish solid (mp 228-229 °C).

$\delta$  9.14 (s, 1H), 8.82 (s, 1H), 7.86 (m, 4H), 7.69 (d,  $J = 8.9$  Hz, 2H), 7.52 (m, 5H), 7.30 (t,  $J = 7.8$  Hz, 2H), 7.00 (t,  $J = 7.3$  Hz, 1H).

(for detailed assignments of peaks see scans of NMR spectra).

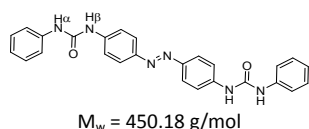
$\delta$  152.15, 152.02, 146.58, 143.10, 139.28, 130.75, 129.34, 128.80, 123.89, 122.20, 118.38, 118.06.

(for detailed assignments of peaks see scans of NMR spectra).

Calc. for C<sub>19</sub>H<sub>17</sub>NO<sub>4</sub> [M+H]<sup>+</sup>: 317.1398, found: 317.1402.

Calc. for **1a** (C<sub>19</sub>H<sub>16</sub>N<sub>4</sub>O<sub>1</sub>): C 72.14, H 5.10, N 17.71, found: C 72.17, H 5.15, N 17.43.

## Host E-1b



The mixture of 4,4'-diaminoazobenzene **3** (1.0 g, 4.7 mmol) and phenyl isocyanate (1.12 mL, 10.3 mmol, 2.2 equiv) was refluxed in anhydrous acetonitrile (20 mL) overnight under argon atmosphere. Then the orange product was filtered off, washed with hot acetonitrile (50 mL) and suspended in diethyl ether (20 mL). After 30 minutes of vigorous stirring the product was filtered off and dried at high vacuum to give receptor **E-1b** (1.77 g, 87 %) as orange powder (mp > 300 °C).

<sup>1</sup>H NMR (500 MHz, DMSO)

$\delta$  9.07 (s, 2H), 8.79 (s, 2H), 7.83 (d,  $J = 9.0$  Hz, 4H), 7.66 (d, 2H), 7.49 (dd,  $J = 8.6, 1.0$  Hz, 3H), 7.30 (dd,  $J = 8.5, 7.5$  Hz, 2H), 7.01 (td,  $J = 7.4, 1.1$  Hz, 2H)

(for detailed assignments of peaks see scans of NMR spectra).

<sup>13</sup>C NMR (125 MHz, DMSO)

$\delta$  152.2, 146.8, 142.4, 139.4, 128.8, 123.5, 122.1, 118.4, 118.1

(for detailed assignments of peaks see scans of NMR spectra).

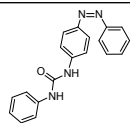
HRMS ESI (m/z)

Calc. for  $C_{26}H_{22}N_6O_4Na$   $[M+Na]^+$ : 473.1702, found: 473.1701.

Anal (%)

Calc. for **1b** ( $C_{26}H_{22}N_6O_4$ ): C 69.32, H 4.92, N 18.66, found: C 69.27, H 4.86, N 18.88.

## Host Z-1a



The ~0.01 M solution of isomer **E-1a** in DMSO was irradiated with UV light (368 nm) over a period of 60 min to give **Z-1a** in 68% yield.

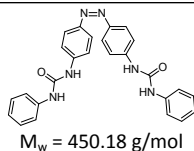
<sup>1</sup>H NMR (200 MHz, DMSO)

$\delta$  8.83 (s, 1H), 8.70 (s, 1H), 7.29 (m, 10H), 6.96 (t,  $J = 7.2$  Hz, 1H), 6.84 (dd,  $J = 9.2, 2.0$  Hz, 4H) (for detailed assignments of peaks see scans of NMR spectra).

<sup>13</sup>C NMR (50 MHz, DMSO)

$\delta$  180.34, 154.03, 152.23, 146.92, 139.34, 129.04, 128.75, 126.82, 122.00, 119.34, 118.26, 117.61. (for detailed assignments of peaks see scans of NMR spectra).

## Host Z-1b



The ~0.01 M solution of isomer **E-1b** in DMSO was irradiated with UV light (368 nm) over a period of 66 min to give **Z-1b** in 50% yield.

<sup>1</sup>H NMR (400 MHz, DMSO)

$\delta$  8.82 (s, 2H), 8.69 (s, 2H), 7.45 – 7.39 (m, 8H), 7.29 – 7.24 (m, 4H), 6.99 – 6.93 (m, 2H), 6.86 (d,  $J = 8.7$  Hz, 4H) (for detailed assignments of peaks see scans of NMR spectra).

<sup>13</sup>C NMR (100 MHz, DMSO)

$\delta$  152.22, 146.83, 142.42, 139.37, 128.79, 123.44, 122.10, 118.37, 118.12

(for detailed assignments of peaks see scans of NMR spectra).

## 1.4 Copies of $^1\text{H}$ and $^{13}\text{C}$ NMR spectra

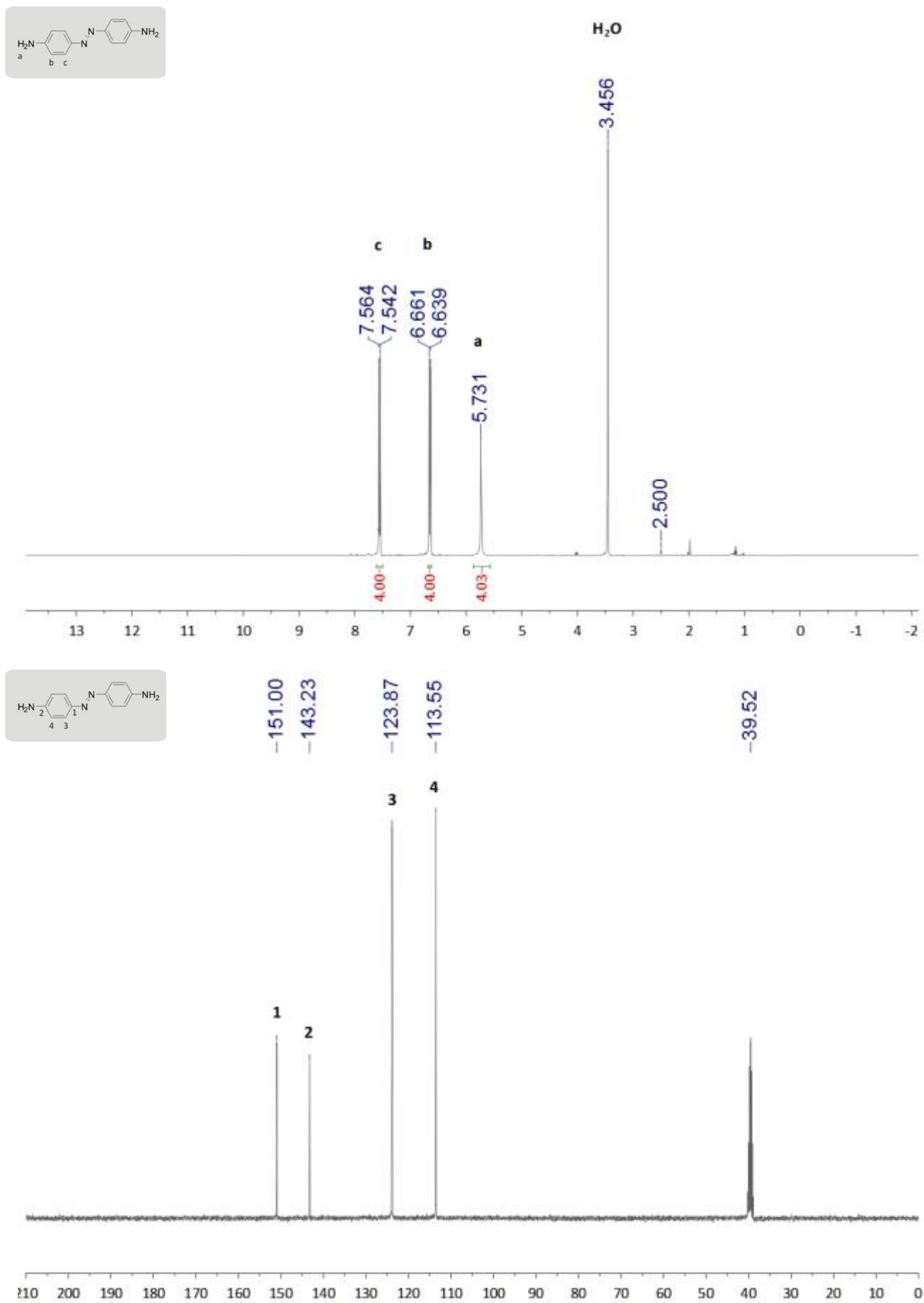


Fig. S1 NMR spectra of compound 3 in DMSO- $d_6$  (400MHz).

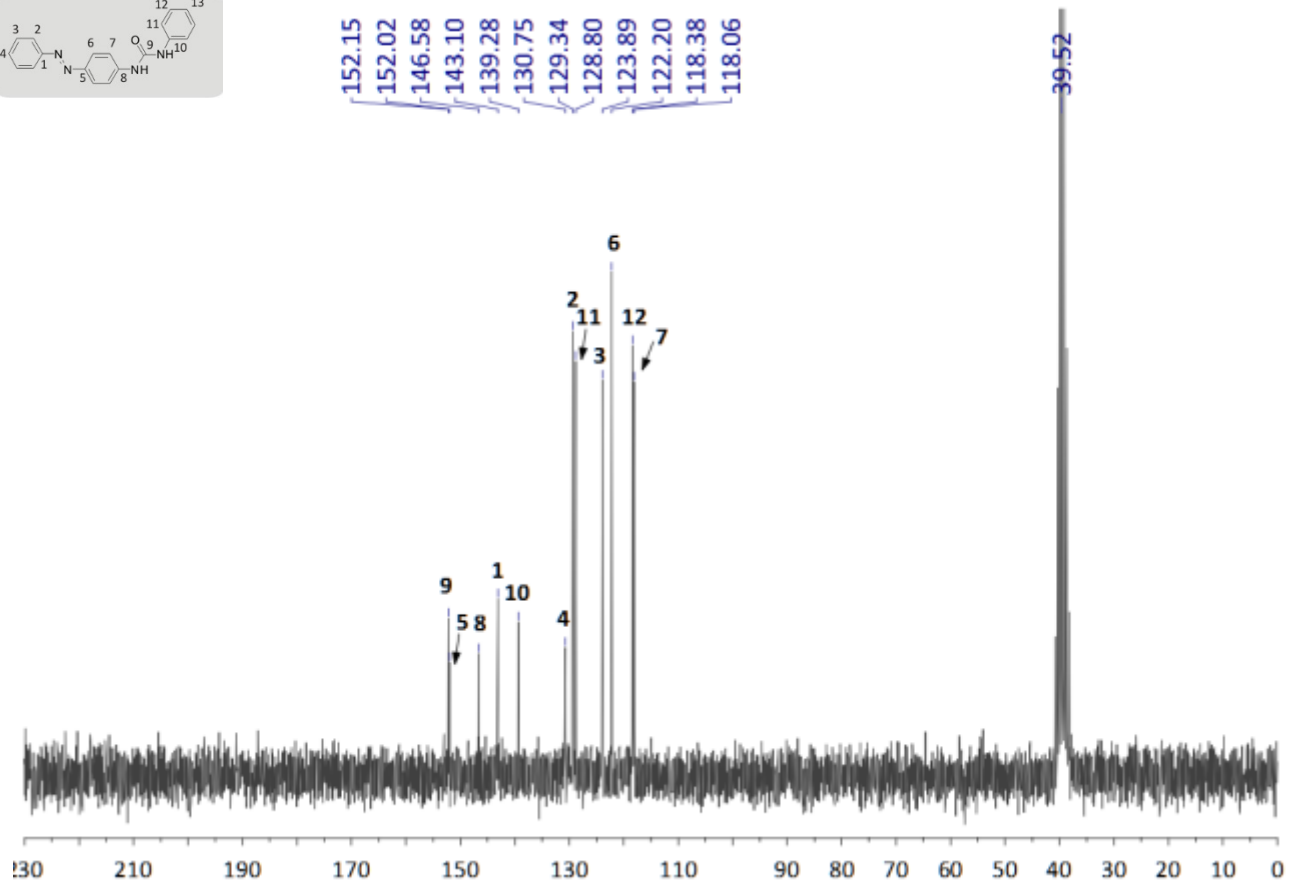
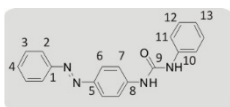
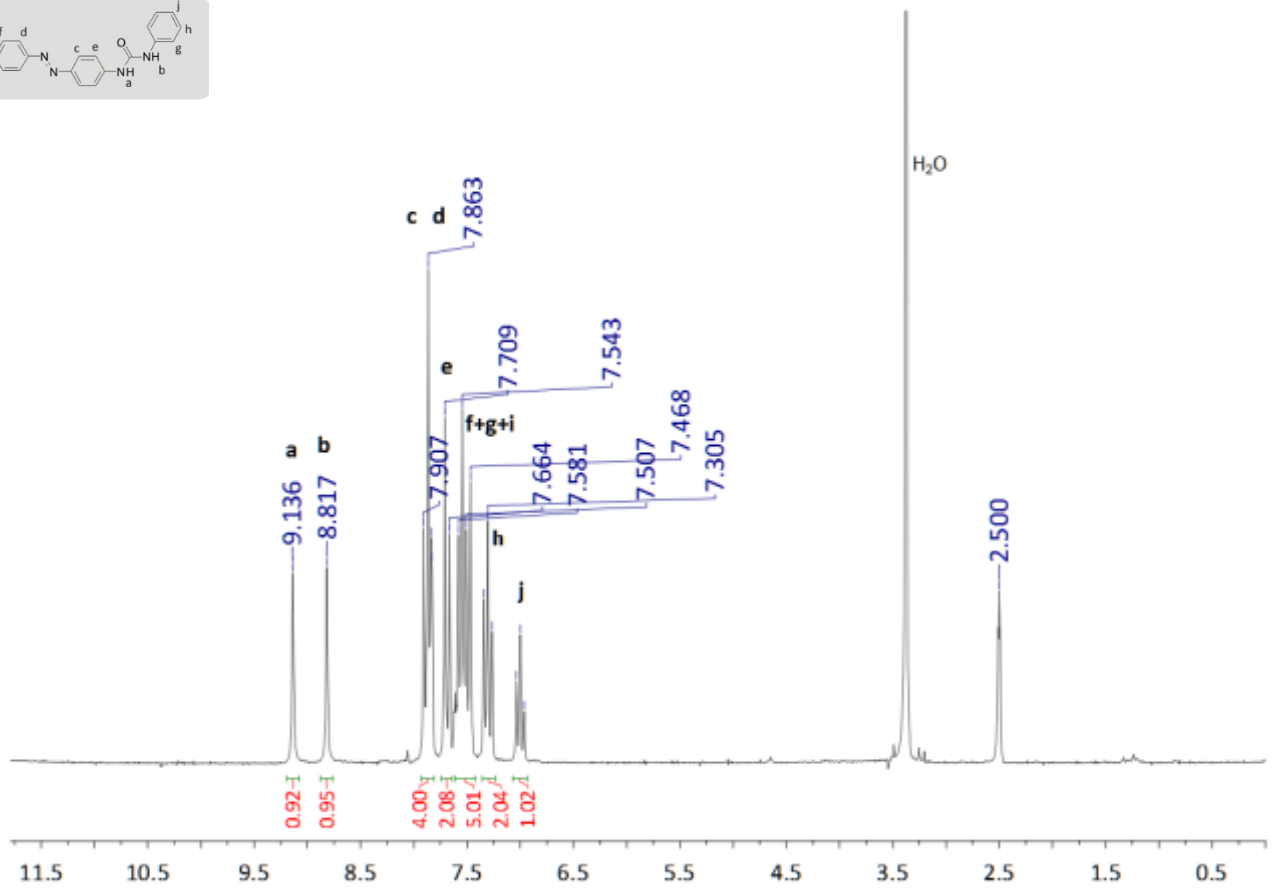
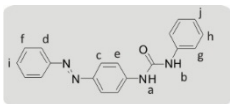
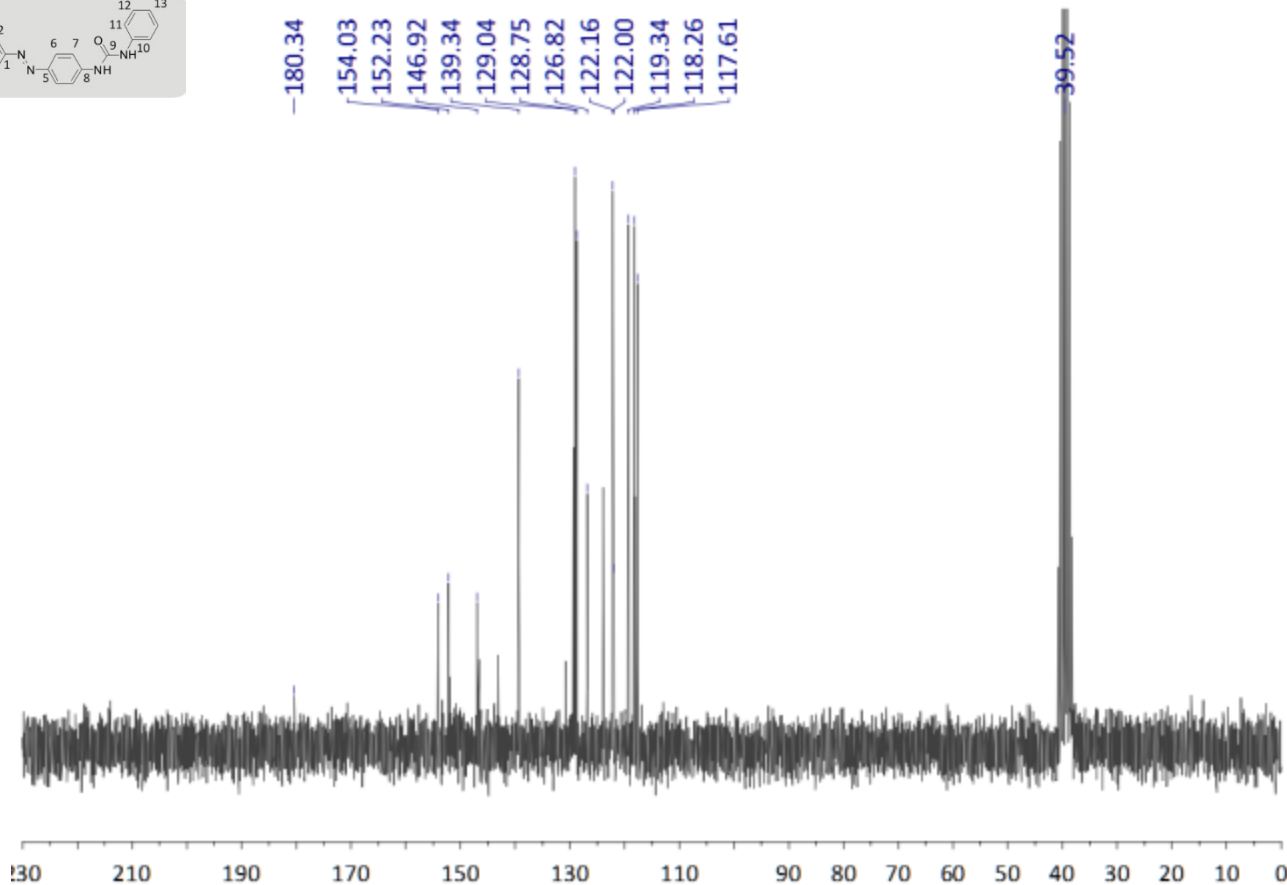
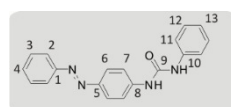
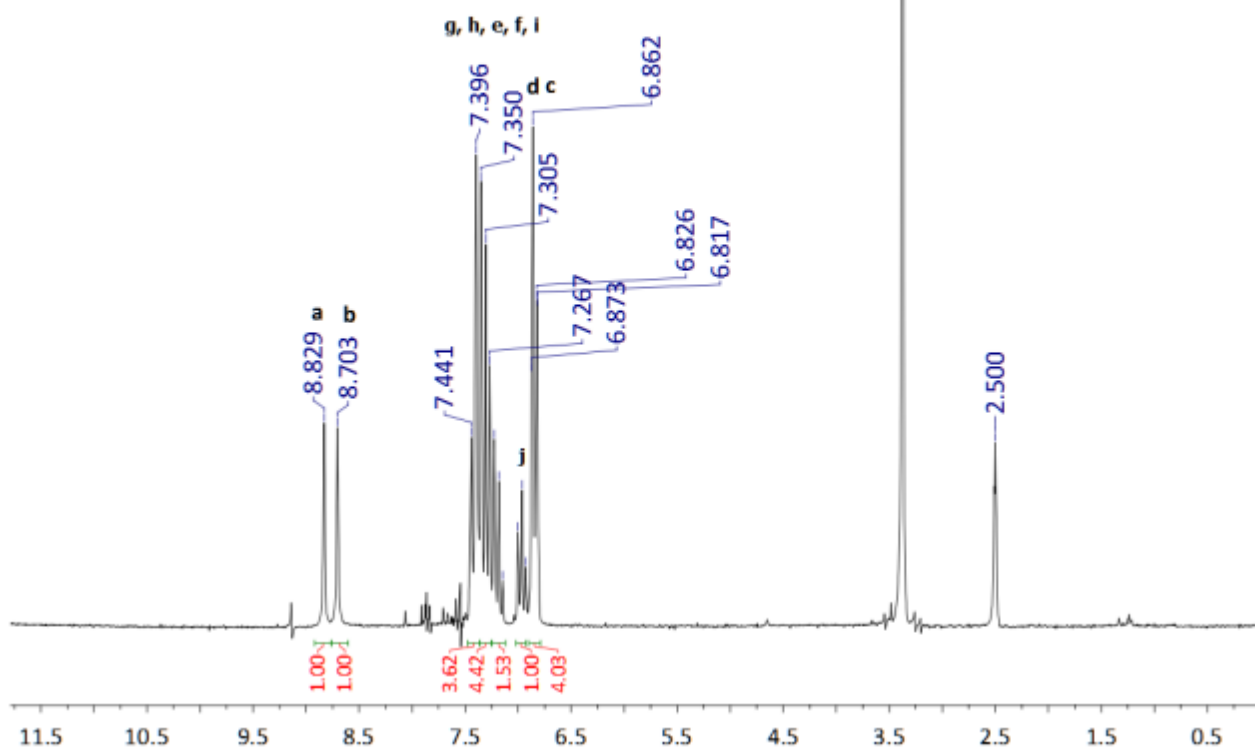
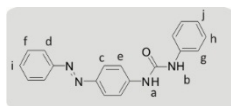


Fig. S2 NMR spectra of compound *E-1a* in  $\text{DMSO-}d_6$  (200MHz).



**Fig. S3** NMR spectra of a mixture of the *E*- and *Z*-**1a** in DMSO-*d*<sub>6</sub> (200MHz), only peak labels of *Z*-**1a** are shown (top) or labeled (bottom).

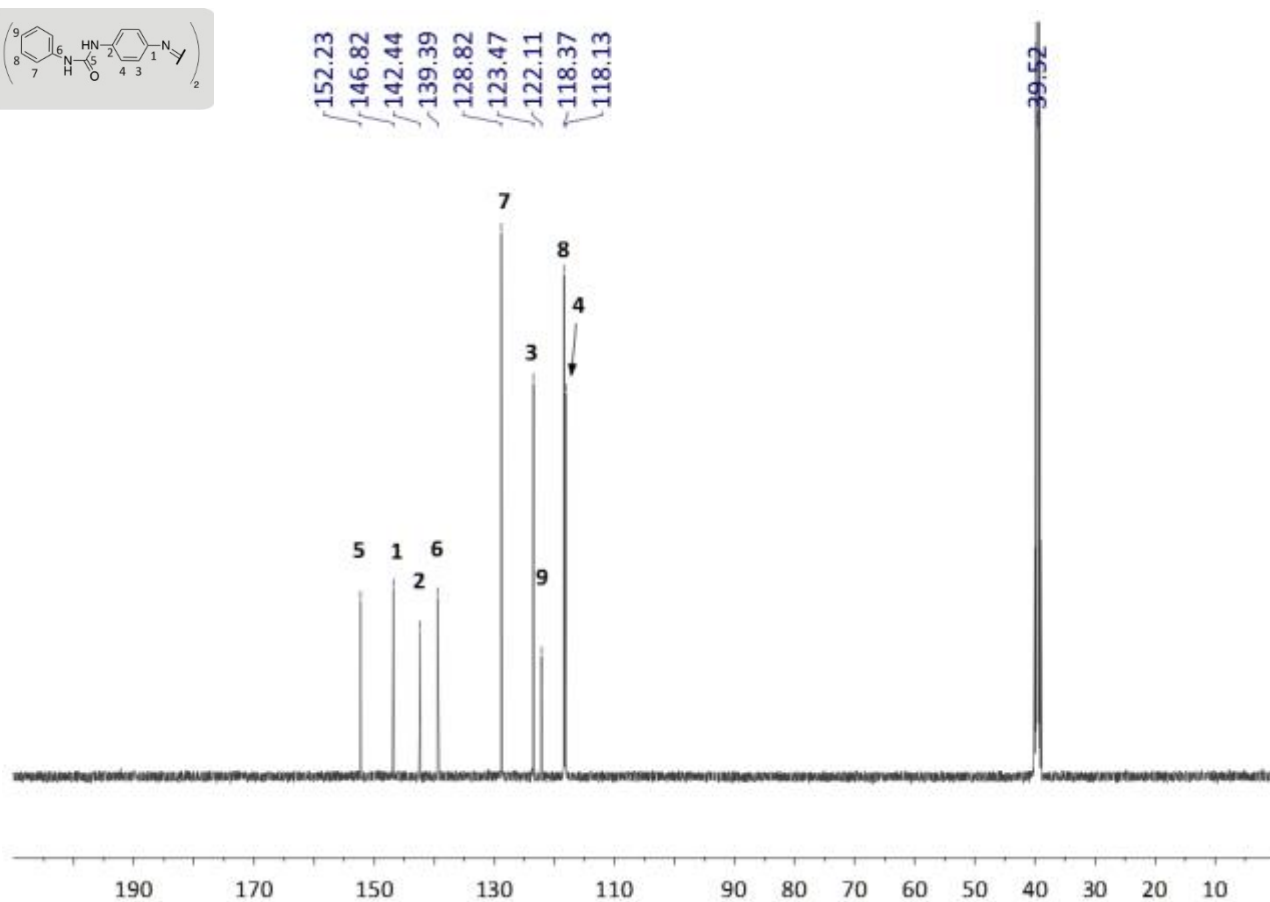
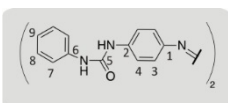
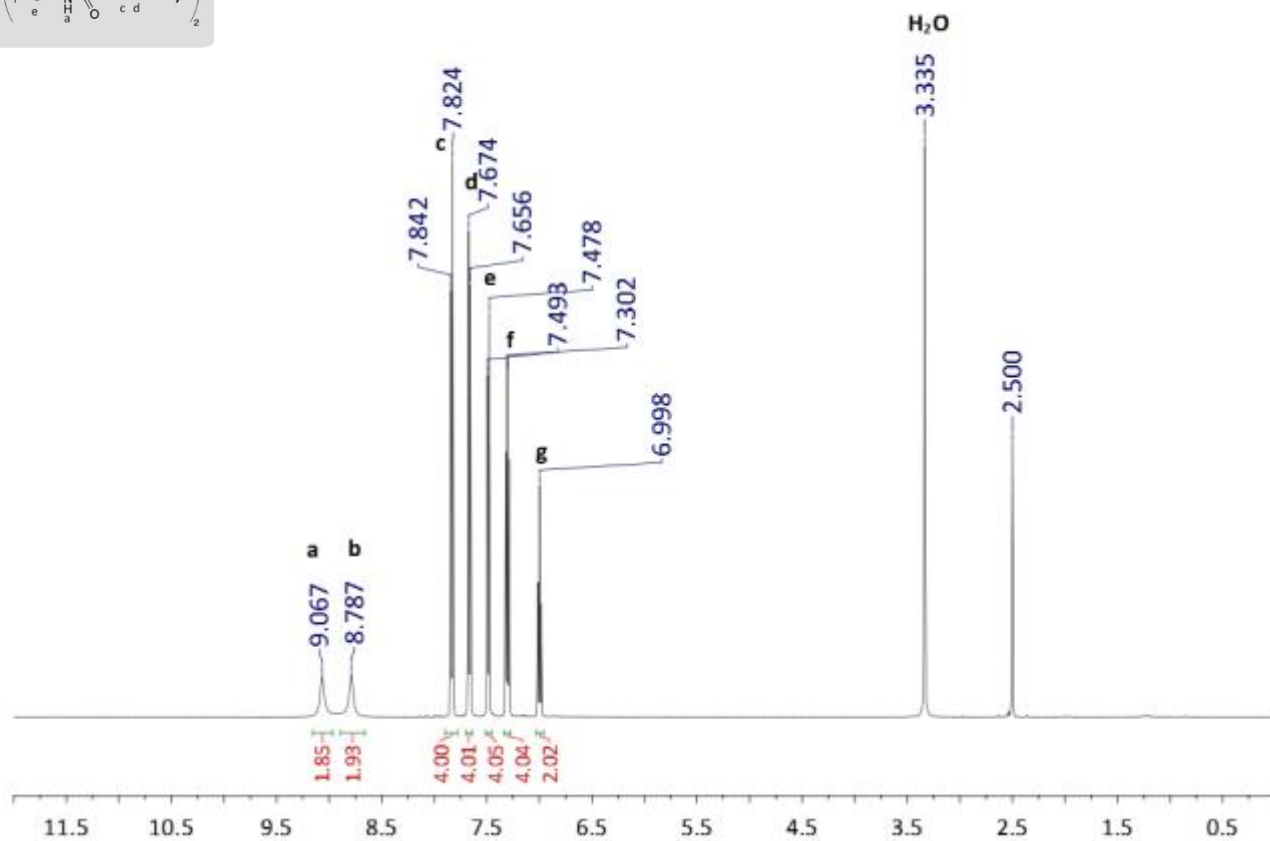
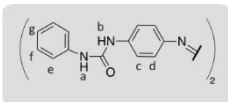


Fig. S4 NMR spectra of compound *E-1b* in DMSO-*d*<sub>6</sub> (500MHz).

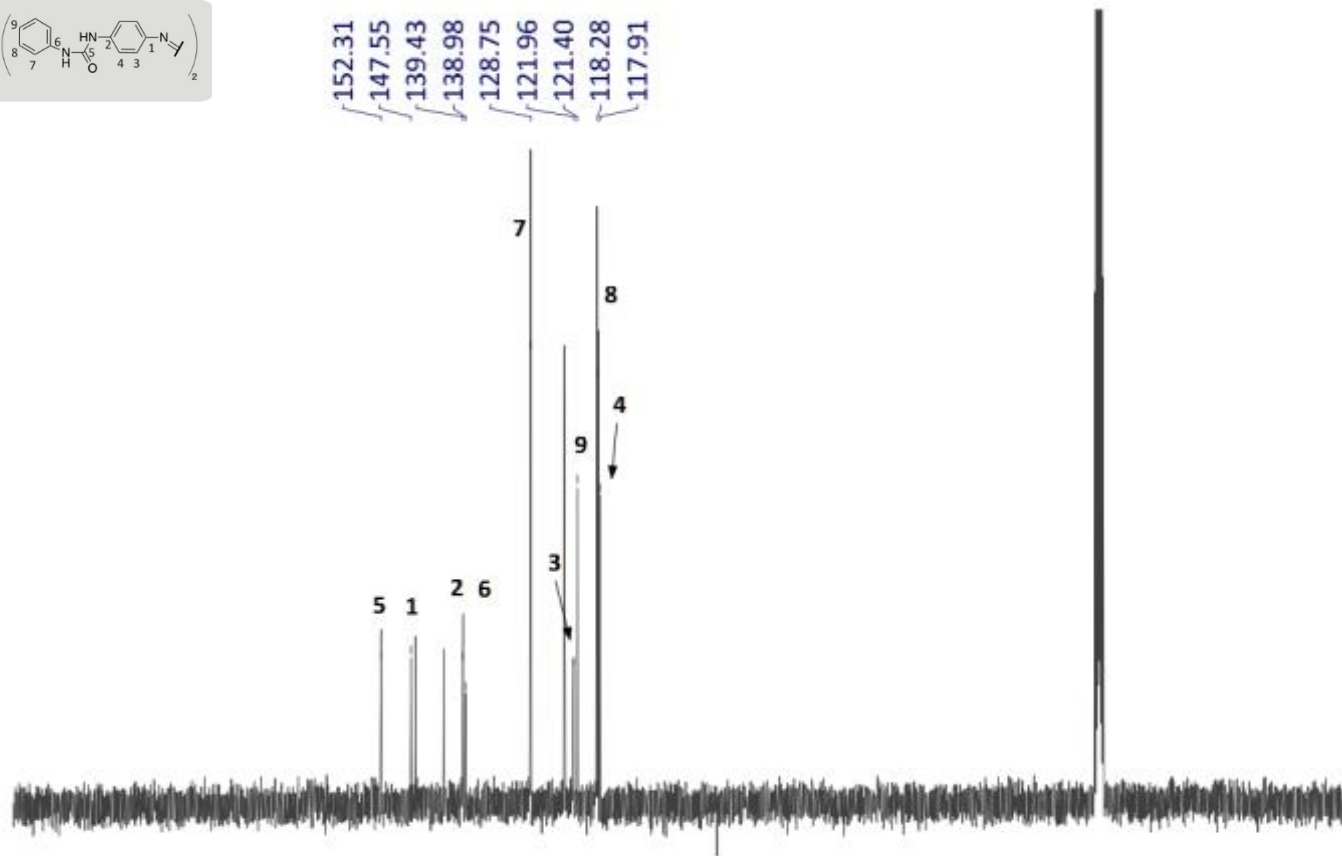
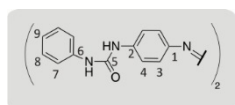
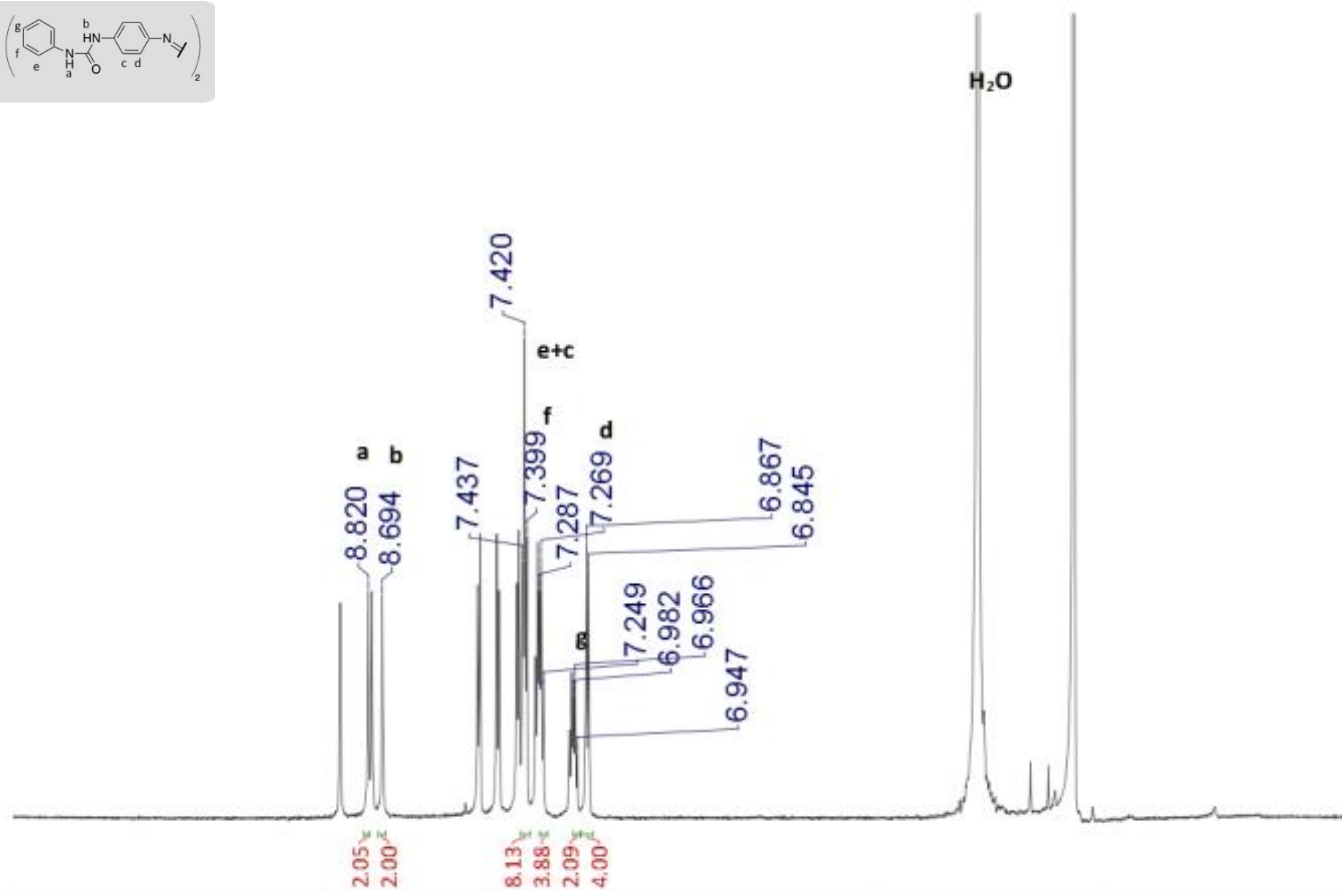
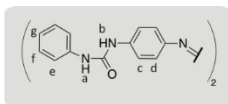


Fig. S5 NMR spectra of a mixture of the *E*- and *Z*-**1b** in DMSO-*d*<sub>6</sub> (400MHz), only peak labels of *Z*-**1b** are shown.



## 2. Binding Studies

### 2.1 General remarks

Commercially available tetrabutylammonium salts were used as a source of anions. Prior to the use, salts were dried for 2 days under high vacuum at 60°C and kept in vacuum over solid tetraphosphorous decoxide ( $P_4O_{10}$ ). HPLC grade water (purchased from Carl Roth GmbH) was added to the commercially available DMSO- $d_6$  of 99.80% isotopic purity (purchased from Euriso-Top, PN D010ES) to obtain the appropriate water concentration.

### 2.2 $^1H$ NMR titration experiments

The DMSO solution of a receptor (ca.  $10^{-2}$  M) was titrated in an NMR tube with the 0.1-0.2 M solution of a respective tetrabutylammonium salt. The solution of the salt contained a certain amount of the receptor in order to keep receptor concentration constant during the titration; 16 to 19 data points were recorded, depending on the shape of the titration curve. However, it was important to choose such volumes of aliquots so that most of the data points could occur in close proximity of the inflection point of the respective titration curve. Such a procedure allows for more precise calculation of the binding constants. Moreover, we took into account the shift changes of all protons present in the receptor and guest molecules. In all cases DMSO- $d_6$  + 0.5%  $H_2O$  was used as a solvent mixture. Titration of pure *E-1* was conducted in the amber NMR tube (Wilmad 527-PP-7, 5 mm diameter, limit 400 MHz) and titration of a mixture of *E-* and *Z-1* was conducted in the quartz NMR tube (Wilmad 535-PP-7QTZ, 5 mm diameter, limit 600 MHz). In the latter case photoisomerisation of *E-1* was carried out before anion was added. A nonlinear curve fitting for 1:1 or 1:2 binding model was carried out with the HypNMR 2008 Software<sup>2,3</sup> and allow the determination of global association constant.<sup>4,5</sup> Importantly, the data analysis for individual proton signals of the molecule reveal the same value of  $K_a$  (in the experimental error), which suggests that the 1:2 (host:guest) model is correct. Additionally to acknowledge complexation stoichiometry, the Job experiments were also conducted.<sup>6,7</sup> Determination of association constants for *Z-1* was carried out using fixed values of association constant for *E-1* obtained during titration of pure *E-1* in darkness. Possible self-association for the host *E-1b* was excluded by additional dilution experiments (data not included), however, for the host *E-1a* weak dimerization was observed, which value ( $K_{dimer}$   $3.3 \pm 1.6 M^{-1}$ ) was included in the subsequent determination of the association constants  $K_a$ .

**Table S1.** The details of  $^1H$  NMR titration experiments for complexes of receptor **1** with TBA-benzoate<sup>[a]</sup>

Host	$C_{Host}$ (M)	$C_{Guest}$ (M)	$K_{a,1}$ ( $M^{-1}$ )	$K_{a,2}$ ( $M^{-1}$ )	$\Delta\delta_{max}$ (ppm)				
					NH $\blacktriangle$	NH $\blacksquare$	Ar $\blacktriangle$	Ar $\blacksquare$	Ar $\blacktriangle$
<i>E-1a</i>	0.01197	0.21045	$1287 \pm 14$	-	3.52	3.44	-0.01	0.27	0.26
<i>Z-1a</i>	0.01197 <sup>[b]</sup>	0.21045	$1127 \pm 11$	-	3.53	3.38	-0.01	-[c]	-[c]
<i>E-1b</i>	0.01079	0.13922	$989 \pm 90$	$341 \pm 29$	3.45	3.40	-0.04	0.28	0.26
<i>Z-1b</i>	0.01337 <sup>[b]</sup>	0.27825	$231 \pm 7$	-	3.65	3.51	-[d]	0.29	-[d]

[a] Titration conducted in DMSO- $d_6$  + 0.5%  $H_2O$  at 298 K; [b] the total host concentration is given for a mixture of *E-* and *Z-1*; [c] overlapping of the  $^1H$  signals upon titration precludes determination of the  $\delta_{max}$ .

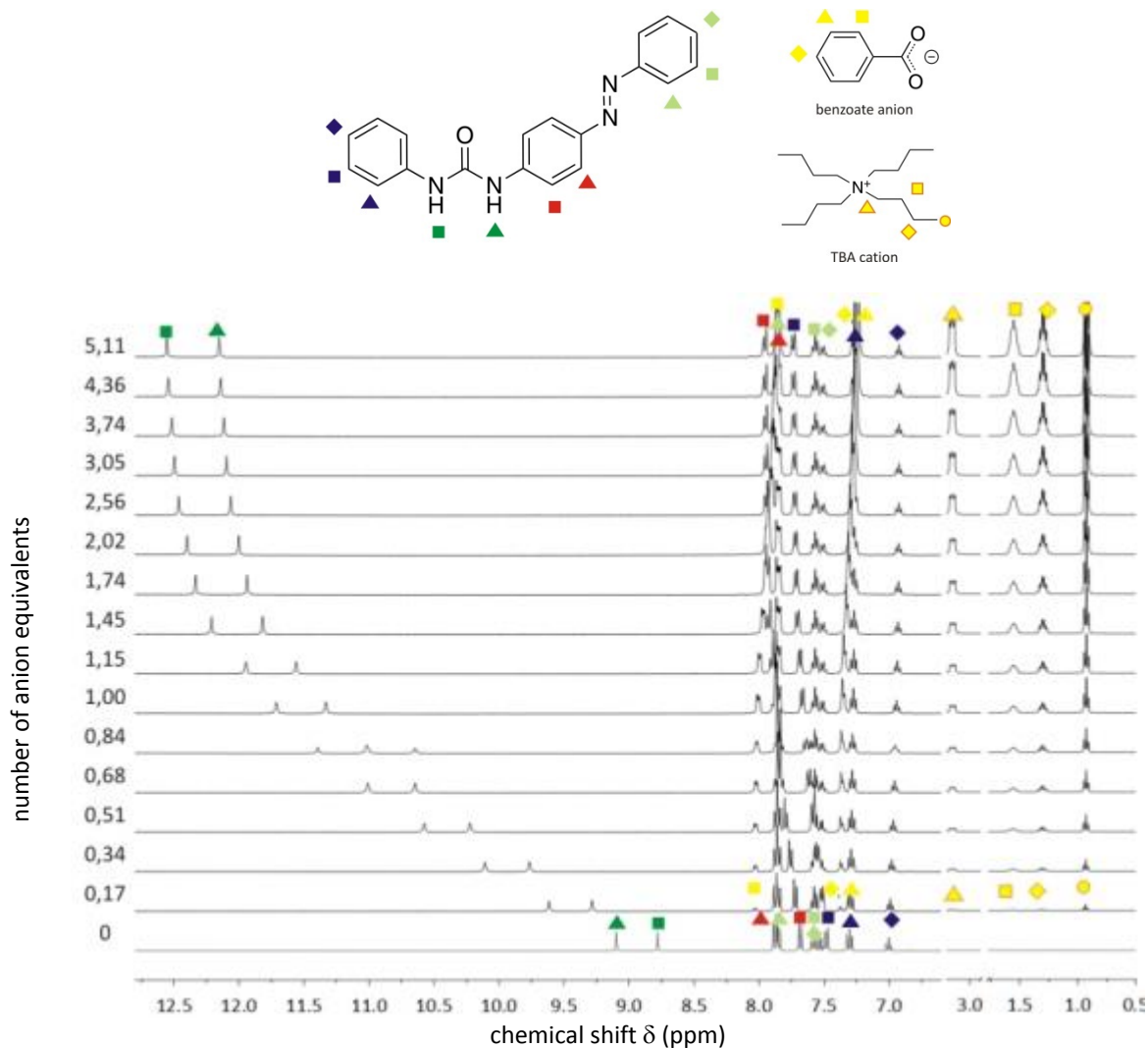


Fig. S6  $^1\text{H}$  NMR spectra of *E-1a* with increasing amount of TBA- $\text{PhCO}_2$

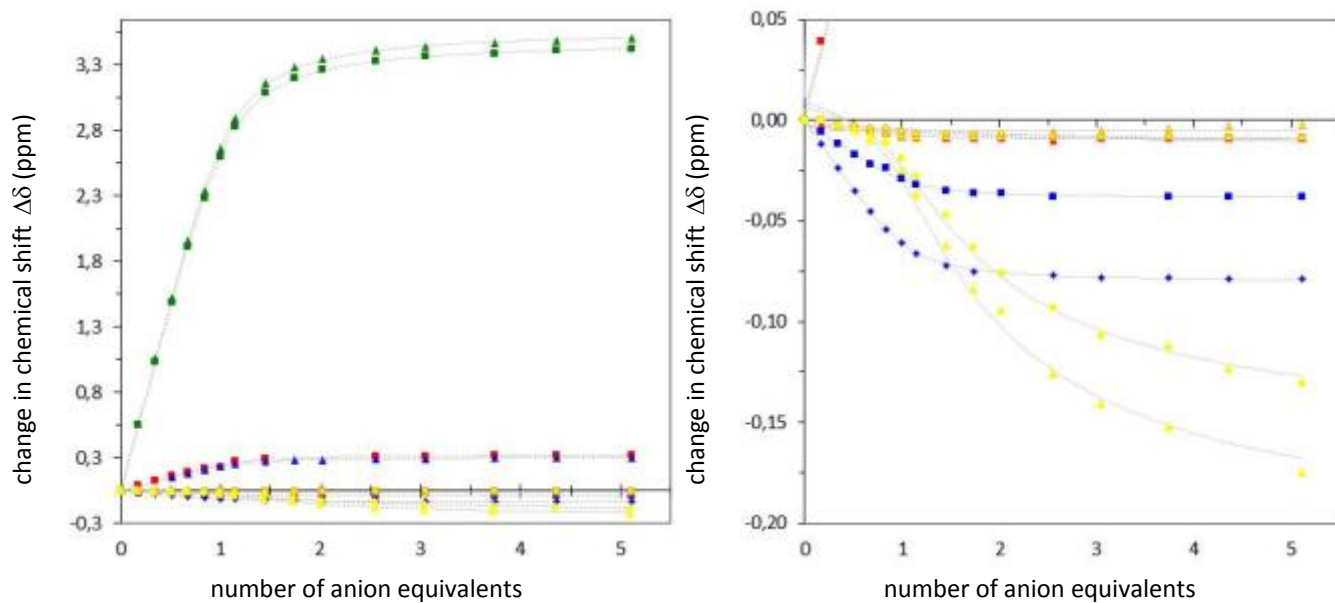


Fig. S7 Changes in chemical shifts and calculated binding isotherms for titration of *E-1a* + TBA- $\text{PhCO}_2$ , magnification of the plot in the range of the small chemical shift changes (right).

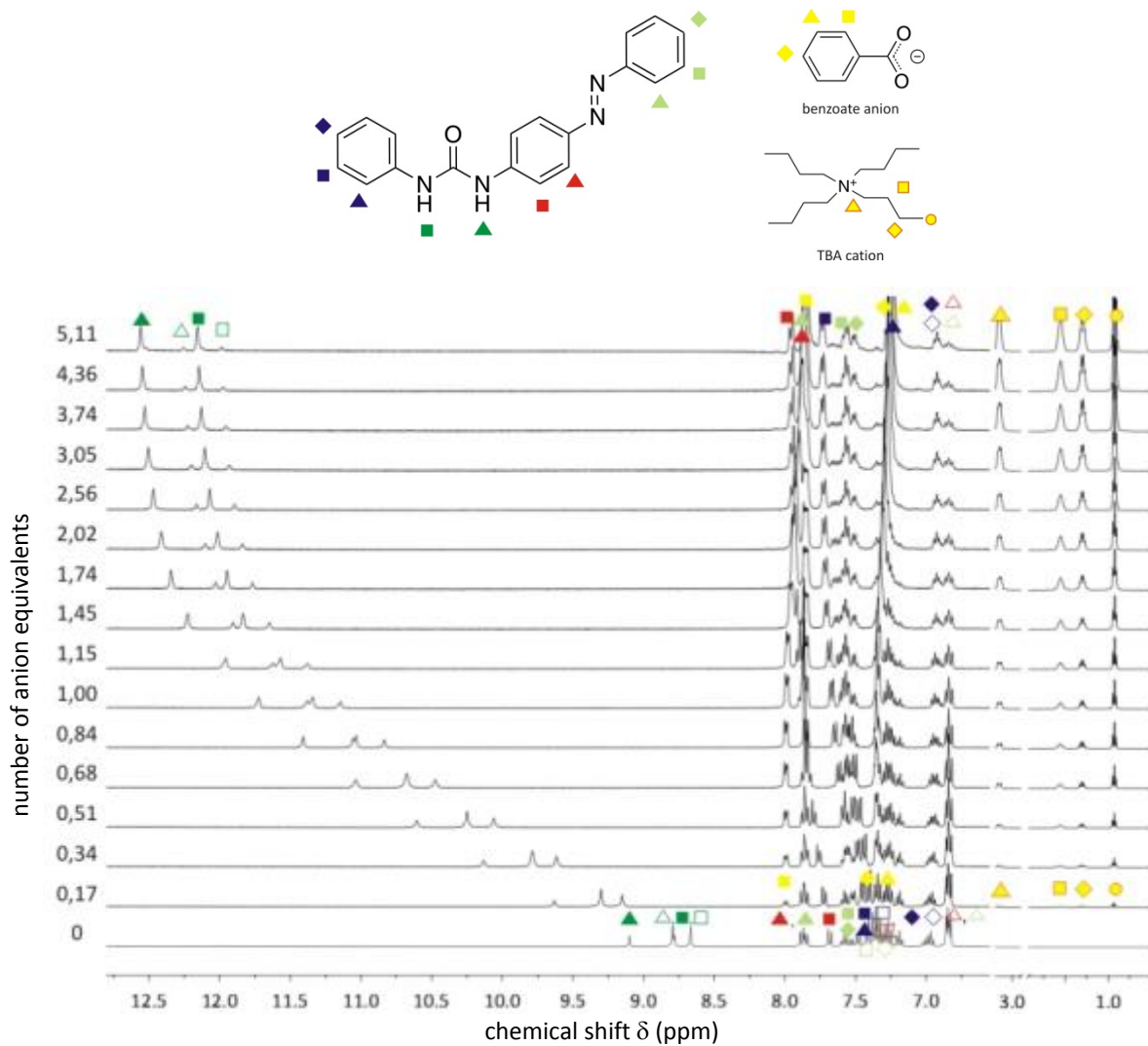


Fig. S8  $^1\text{H}$  NMR spectra of *EZ-1a* with increasing amount of TBA-  $\text{PhCO}_2$

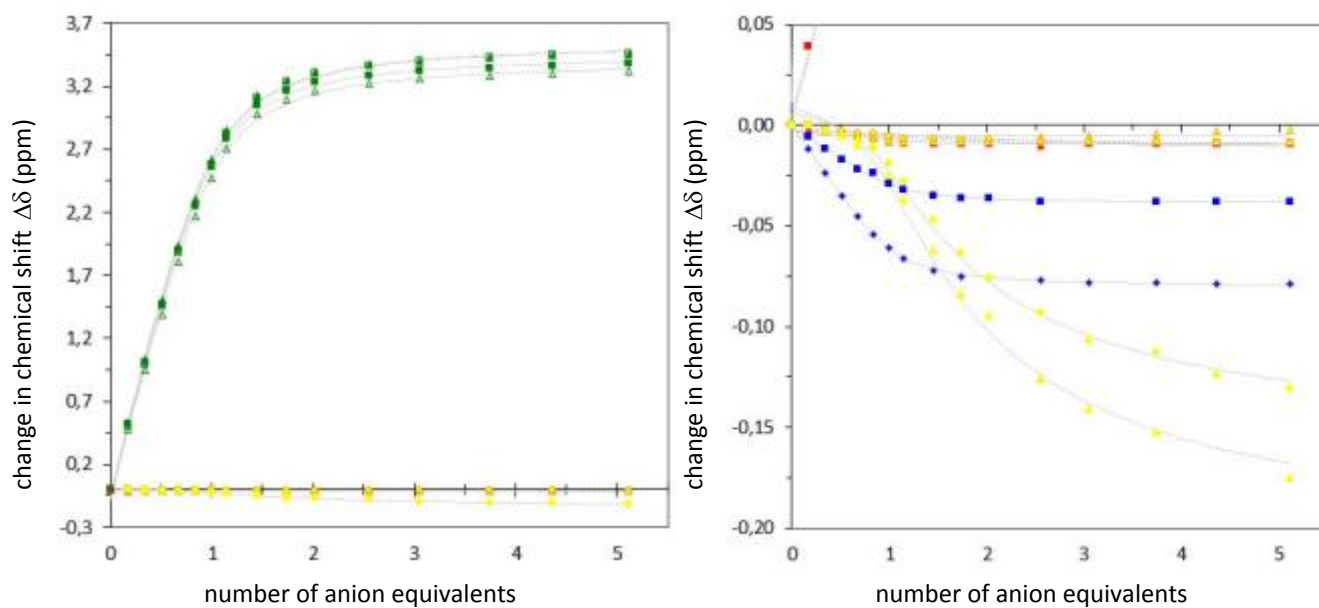


Fig. S9 Changes in chemical shifts and calculated binding isotherms for titration of *EZ-1a* + TBA-  $\text{PhCO}_2$ , magnification of the plot in the range of the small chemical shift changes (right).

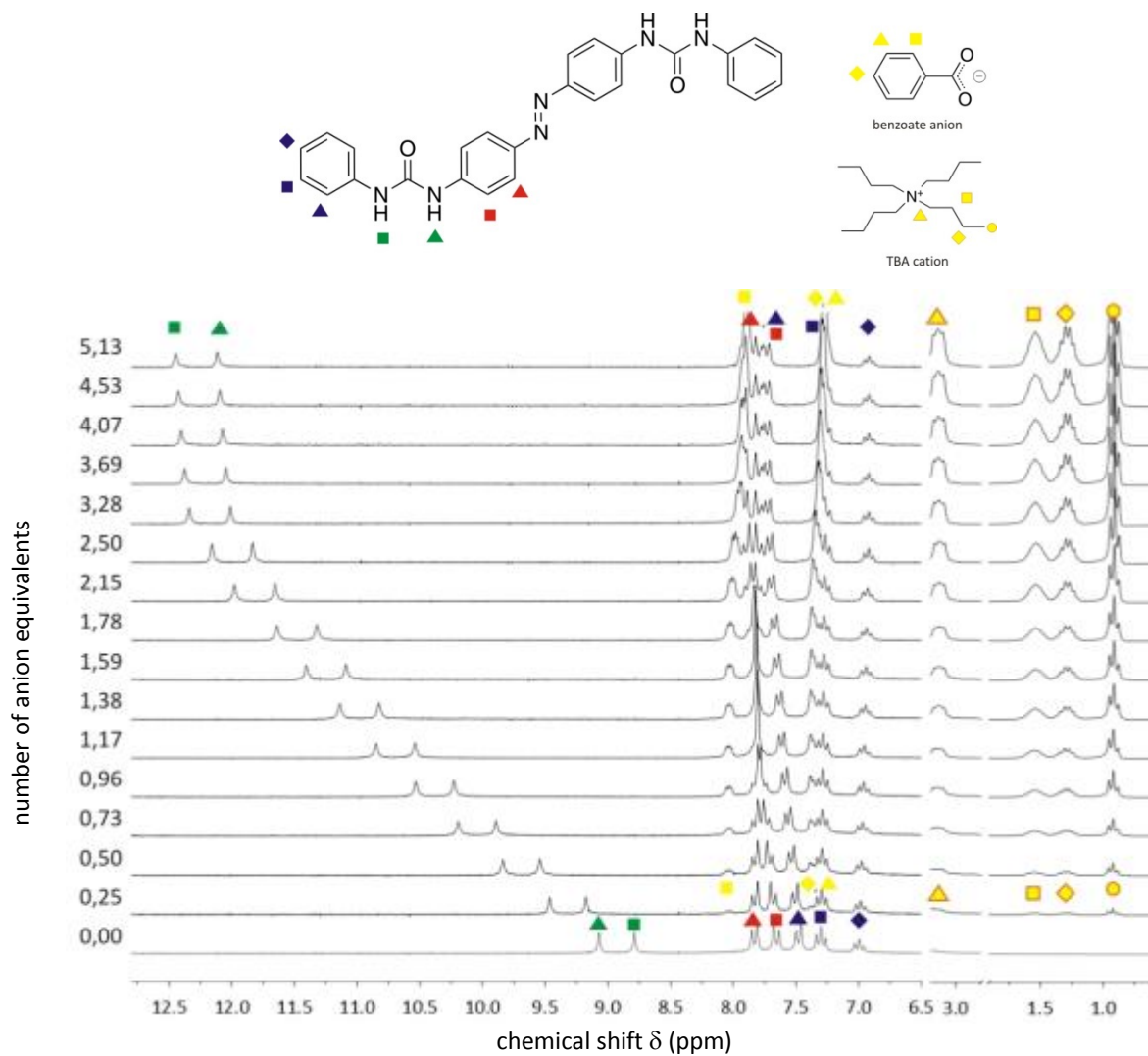


Fig. S10  $^1\text{H}$  NMR spectra of *E-1b* with increasing amount of TBA- $\text{PhCO}_2$

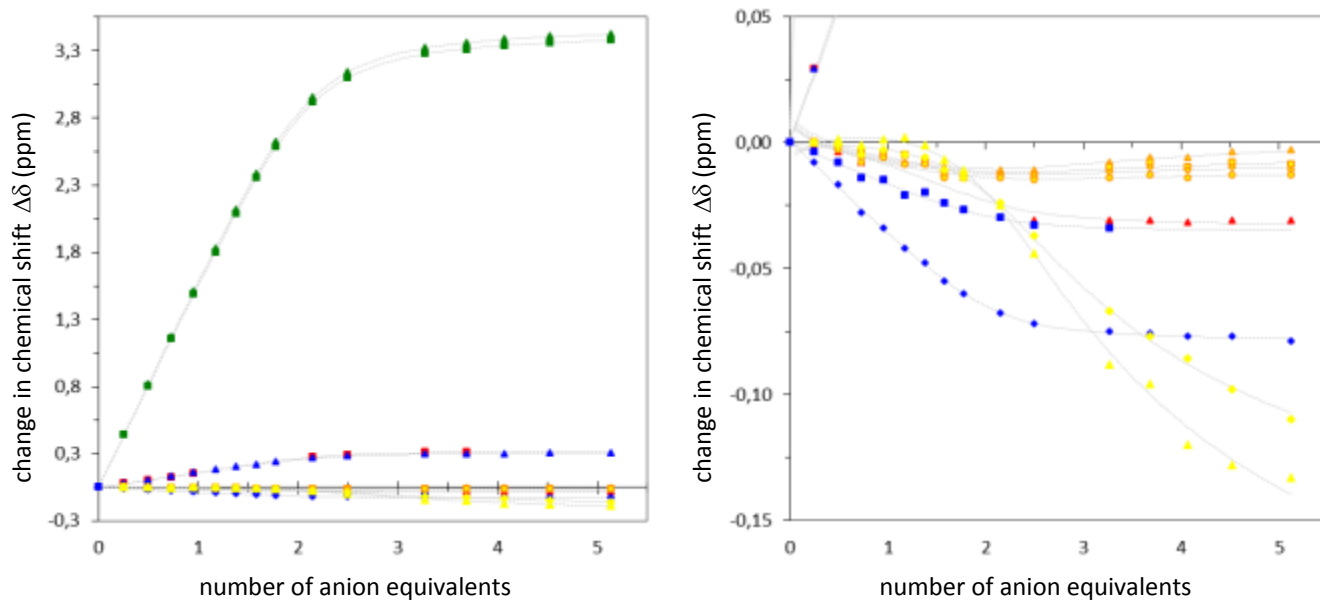


Fig. S11 Changes in chemical shifts and calculated binding isotherms for titration of *E-1b* + TBA-  $\text{PhCO}_2$ , magnification of the plot in the range of the small chemical shift changes (right).

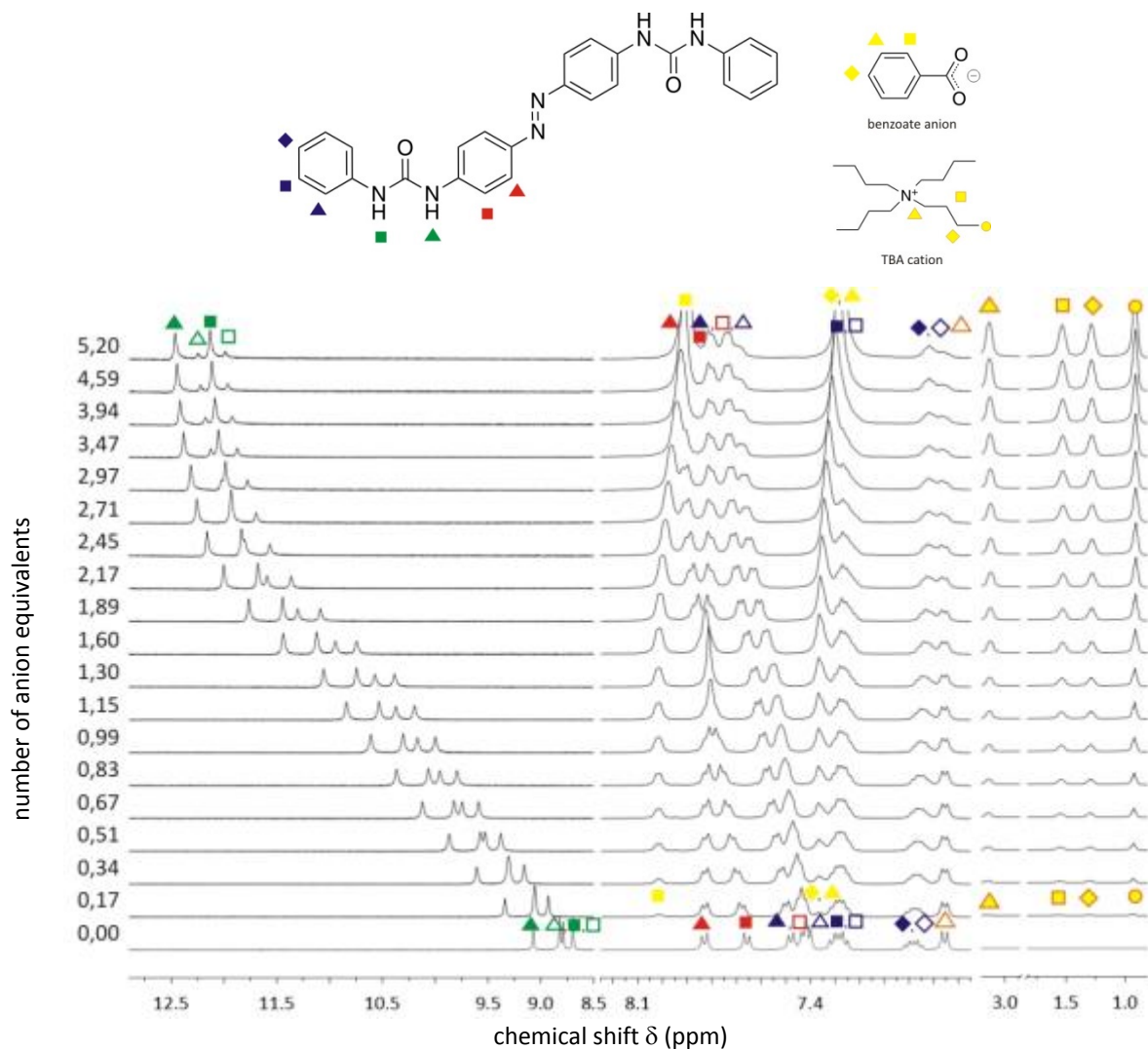


Fig. S12  $^1\text{H}$  NMR spectra of *EZ-1b* with increasing amount of TBA-  $\text{PhCO}_2$

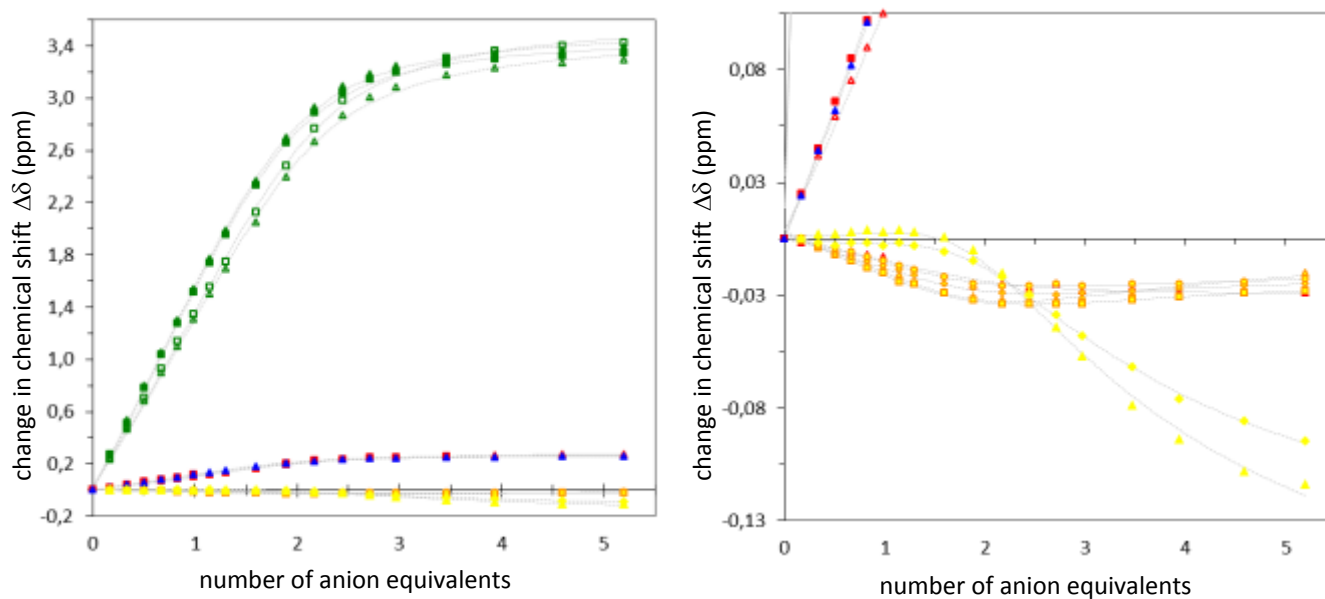


Fig. S13 Changes in chemical shifts and calculated binding isotherms for titration of *EZ-1b* + TBA-  $\text{PhCO}_2$ , magnification of the plot in the range of the small chemical shift changes (right).

## 2.3 $^1\text{H}$ NMR Job plot experiments

0.40 mL of the  $2 \cdot 10^{-2}$  M receptor solution was titrated in the NMR tubes with 50  $\mu\text{l}$  aliquots of the equimolar solution of the respective tetrabutylammonium salt, to the point of 1:1 receptor:anion ratio. Similarly, the anion solution was titrated with the receptor solution. Approximately 16-17 data points were recorded to obtain respective Job plots.

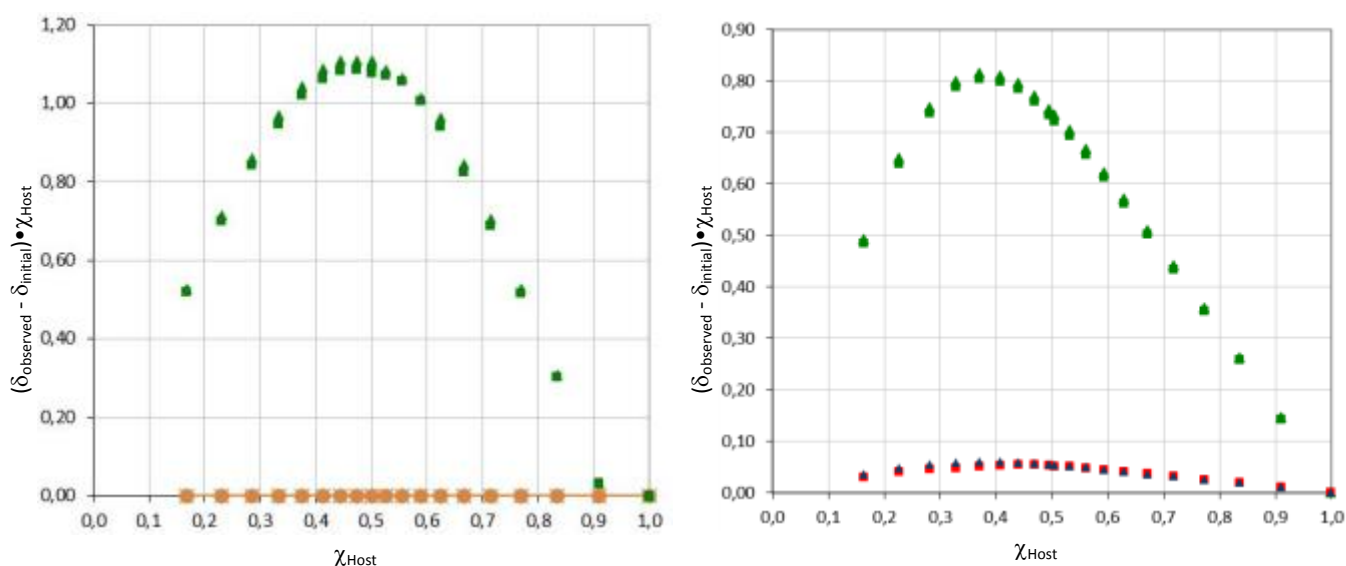


Fig. S14 Job Plots for hosts *E-1a* (left) and *E-1b* (right) upon decreasing molar fraction of TBA-BzO.

## 2.4 DFT Calculations

All calculations were performed in the gas-phase and DMSO (employing implicit SM8 solvation model)<sup>8</sup> using Spartan'10 Parallel for Windows software package.<sup>9</sup> Commonly used exchange-correlation functional B3LYP<sup>10</sup> with proved to be reasonably-well in calculations of many neutral azobenzene derivatives<sup>11</sup> due to the lack of the dispersion component is inadequate to properly describe the hydrogen bonds and London dispersion forces associated with anion binding. Therefore, in order to improve the accuracy of calculations while remaining within acceptable computational cost, we used the density functional theory (DFT) method with long-range dispersion corrected hybrid functional  $\omega\text{b97x-d}$ ,<sup>12,13</sup> combined with the 6-31+G\* basis set.<sup>14</sup> This functional proved to be robust and accurate in describing noncovalent supramolecular complexes.<sup>15-20</sup> Initial accuracy test for  $\omega\text{b97x-d}$ , B3LYP, and EDF2<sup>20,21</sup> functionals in comparison to available X-ray structures of the *E*- and *Z*-isomers of an azobenzene (AB) clearly demonstrate that  $\omega\text{b97x-d}$  functional gave results very similar to X-ray data (at least for *E*-AB), whereas B3LYP and EDF2 functionals slightly overestimate the bond distance between azo nitrogen atoms (Table S2). Nevertheless, contrary to X-ray data all studied functionals predicted shorter distance of the azo linkage for *Z*-AB than for *E*-AB. Disruption of the system  $\pi$ -electron conjugation in the *Z* isomer should increase the double bond character of the N=N bond and observed elongation of this bond in the solid state could be attributed to crystal packing forces.

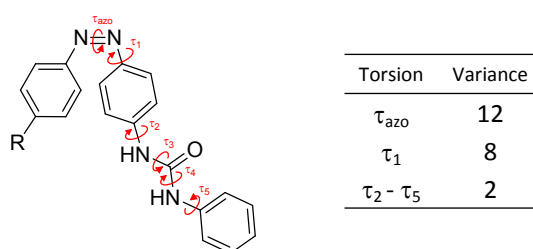
Analysis of the values of the HOMO-LUMO gap (associated with absorption frequency of the  $n\text{-}\pi^*$  transition) in Table S2 demonstrate that  $\omega\text{b97x-d}$  functional is unable to correctly predict these properties (although graphical representation of MOs and trend of their energies changes upon anion binding are correct, see section 2.5). Moreover, subsequent attempts to calculate transient spectra for a more complex molecules (e.g. hosts *E-1*) do not converge (in a reasonable time). Therefore, we decided to carry out additional calculations at the DFT/EDF2/6-31G\* level of theory which successfully predict these properties for comparable minimum energy geometries (B3LYP gave comparable results, however, the parameterized EDF2 functional is significantly faster in calculations of transient spectra).

**Tab. S2** Accuracy test for various DFT functionals in comparison with X-ray structures for azobenzene (AB)<sup>[a]</sup>

No.	Compound	Level of theory	$\Delta E_{Z,E}$ (kJ·mol <sup>-1</sup> )	$d_{N=N}$ (Å)	$\angle_{\text{dih,C-N=N-C}}$ (°)	$\mu$ (D)	HOMO-LUMO gap (eV)
1	<i>E</i> -AB <sup>b</sup>			1.247(2)	180.0(2)		
2	<i>Z</i> -AB <sup>c</sup>	n.a.	n.a.	1.253(4)	53.0(3)	n.a.	n.a.
3	<i>E</i> -AB	$\omega$ b97x-d/6-31G*	50.4	1.249	-180.0	0.00	-7.8
4	<i>Z</i> -AB	$\omega$ b97x-d/6-31G*		1.242	-6.4	3.37	-7.9
5	<i>E</i> -AB	$\omega$ b97x-d/6-31+G*	52.3	1.246	-180.0	0.00	-7.7
6	<i>Z</i> -AB	$\omega$ b97x-d/6-31+G*		1.242	-6.2	3.50	-7.8
7	<i>E</i> -AB	EDF2/6-31G*	63.8	1.257	180.0	0.00	-3.6
8	<i>Z</i> -AB	EDF2/6-31G*		1.246	-10.4	3.24	-3.5
9	<i>E</i> -AB	EDF2/6-31+G*	66.0	1.255	180.0	0.00	-3.6
10	<i>Z</i> -AB	EDF2/6-31+G*		1.246	-9.9	3.41	-3.4
11	<i>E</i> -AB	B3LYP/6-31G*	64.2	1.260	180.0	0.00	-4.0
12	<i>Z</i> -AB	B3LYP/6-31G*		1.250	-9.5	3.22	-3.8
13	<i>E</i> -AB	B3LYP/6-31+G*	66.6	1.258	180.0	0.00	-3.9
14	<i>Z</i> -AB	B3LYP/6-31+G*		1.249	-9.3	3.40	-3.7

[a] All calculations were performed in the gas-phase, all values are given for the lowest energy structures, n.a. – not applicable; [b] X-ray structure, data from ref. <sup>21,22</sup>; [c] X-ray structure, data from ref. <sup>23</sup>

To find lowest-energy structures of both free receptors and their complexes with anions conformational analysis as implemented in Spartan was performed. Briefly, fast semi-empirical model PM6 was used to find 64 lowest-energy conformers of both *E*- and *Z*-isomers of the corresponding compound from the set of ~20000 conformers generated for the given torsion angles (Fig. S15).

**Fig S15** Torsions and variances of the torsion angles used to generate conformers (**1a**: R=H, **1b**: R=PhNHCONH)

Energies of the remaining conformers were corrected at the DFT/ $\omega$ b97x-d/6-31G\*/SM8-DMSO level of theory and duplicates and nearly identical rotamers were removed. The geometry of the 3-4 best conformers were then optimized without any restraints at the DFT/ $\omega$ b97x-d/6-31+G\*/SM8-DMSO level of theory (Tab. S3). The harmonic vibrational frequencies were calculated using DFT/EDF2/6-31G\*/SM8-DMSO level of theory in order to confirm whether the obtained geometries corresponded to the true energetic minima (no imaginary frequencies). Initial trials demonstrate that BSSE error is relatively small (< 8 kJ·mol<sup>-1</sup>), at least in the gas-phase, for all compound studied.

The calculations predicts that *Z*-**1a** isomer is higher in energy by 60 kJ/mol than *E*-**1a**, whereas for *Z*-**1b** vs *E*-**1b** the difference is slightly lower (58 kJ/mol). The binding energy  $\Delta E_{\text{bind}}$  between complexes of *E*-**1a** and *Z*-**1a** with a benzoate anion is predicted to be similar; however, for *Z*-**1b** host it is much lower than for *E*-**1b**. Both isomers of **1a** as well as *E*-**1b** bind the benzoate anion with two strong hydrogen bonds derived from the urea groups and two weaker C-H... $\pi$  bonds originating from the aromatic substituents. In the case of *Z*-**1b**, the anion is bound exclusively by the four adjacent urea protons in the cavity formed between the benzene rings. However, the interaction energy for the structure where the benzoate anion is bound outside the cavity is only slightly smaller, which indicates the high deformation energy of the latter conformation.

Nonetheless, in contrast to free hosts **1**, complexes of **Z-1** with benzoate exhibit a reduced dipole moment compared with the corresponding *E* isomers. As has been mentioned above,  $\omega$ b97x-d functional failed to predict reliable energies for MOs, however, trend in changes of their energies is similar to that predicted by EDF2 functional, i.e. anion binding raise the energy of the *n* and  $\pi$  MOs, and decrease the energy of  $\pi^*$  MOs. As a consequence, the corresponding *n*- $\pi^*$  and  $\pi$ - $\pi^*$  bands are blue and red shifted, respectively, however, this effect is more pronounced for host **1a** than for **1b** (Tab. S4).

**Tab. S3** Energy difference between *Z* and *E* isomer, geometrical data, dipole moments, and interaction energy ( $\Delta E_{\text{int.}}$ ) for structures of hosts **1** and their benzoate complexes calculated at different DFT level of theory<sup>[a]</sup>

No.	Compound	$\Delta E_{Z,E}$ (kJ·mol <sup>-1</sup> )	$d_{N=N}$ (Å)	$\angle_{\text{dih,C-N=N-C}}$ (°)	$d_{\text{urea-centroids}}$ (Å)	$\mu$ (D)	$\Delta E_{\text{int.}}$ (kJ·mol <sup>-1</sup> )
Level of theory: $\omega$ b97x-d/6-31+G*/SM8-DMSO							
1	<i>E-1a</i>	59.8	1.250	-179.79	n.a.	5.91	n.a.
2	<i>Z-1a</i>		1.245	-7.76		7.20	
3	<i>E-1a</i> ⊃PhCO <sub>2</sub> <sup>-</sup>	72.8	1.254	-179.75	n.a.	8.76	-105
4	<i>Z-1a</i> ⊃PhCO <sub>2</sub> <sup>-</sup>		1.247	-8.22		7.66	-106
5	<i>E-1b</i>	58.5	1.250	-179.64	13.97	1.62	n.a.
6	<i>Z-1b</i>		1.243	-8.22	7.78	8.34	
7	<i>E-1b</i> ⊃PhCO <sub>2</sub> <sup>-</sup>	54.3	1.252	-179.57	13.74	27.67	-96
8	<i>Z-1b</i> ⊃PhCO <sub>2</sub> <sup>-</sup> [b]		1.250	-3.56	7.62	10.09	-100
9	<i>Z-1b</i> ⊃PhCO <sub>2</sub> <sup>-</sup> [c]		1.246	-6.83	7.58	7.88	-95
Level of theory: EDF2/6-31G*/SM8-DMSO							
10	<i>E-1a</i>	72.9	1.266	179.94	n.a.	6.61	n.a.
11	<i>Z-1a</i>		1.256	-11.91		10.08	
12	<i>E-1a</i> ⊃PhCO <sub>2</sub> <sup>-</sup>	72.8	1.266	-179.90	n.a.	7.09	-104
13	<i>Z-1a</i> ⊃PhCO <sub>2</sub> <sup>-</sup>		1.257	-11.83		7.36	-104
14	<i>E-1b</i>	75.7	1.268	-179.77	13.70	11.12	n.a.
15	<i>Z-1b</i>		1.259	-13.72	11.22	13.50	
16	<i>E-1b</i> ⊃PhCO <sub>2</sub> <sup>-</sup>	109.6	1.269	179.54	13.94	26.62	-103
17	<i>Z-1b</i> ⊃PhCO <sub>2</sub> <sup>-</sup> [b]		1.261	-6.96	7.86	9.97	-70
18	<i>Z-1b</i> ⊃PhCO <sub>2</sub> <sup>-</sup> [c]		1.260	13.79	11.17	19.97	-101

[a] Values for energy minimized structures in the SM8 DMSO solvent model,  $d_{\text{urea}}$  reflects the distance between centroids of the two adjacent urea groups, n.a. – not applicable; [b] anion bound by both urea group; [c] anion bound exclusively by one urea group

**Tab. S4** Energy levels of the MOs orbitals calculated at DFT/EDF2/6-31G\*/SM8-DMSO level of theory.

No.	Compound	Molecular orbital (eV)			Transition			
		<i>n</i>	$\pi$	$\pi^*$	<i>n</i> - $\pi^*$ (eV)	<i>n</i> - $\pi^*$ (nm)	$\pi$ - $\pi^*$ (eV)	$\pi$ - $\pi^*$ (nm)
1	<i>E-1a</i>	-6.12	-5.38	-2.38	3.74	332	3.00	413
2	<i>E-1a</i> ⊃PhCO <sub>2</sub> <sup>-</sup>	-6.00	-5.17	-2.28	3.72	333	2.89	429
3	<i>Z-1a</i>	-5.31	-5.75	-2.22	3.09	401	3.53	351
4	<i>Z-1a</i> ⊃PhCO <sub>2</sub> <sup>-</sup>	-5.58	-5.13	-2.13	3.45	359	3.00	413
5	<i>E-1b</i>	-6.02	-5.12	-2.25	3.77	329	2.87	432
6	<i>E-1b</i> ⊃PhCO <sub>2</sub> <sup>-</sup>	-5.93	-4.97	-2.15	3.78	328	2.82	440
7	<i>Z-1b</i>	-6.33	-5.01	-2.19	4.14	300	2.82	440
8	<i>Z-1b</i> ⊃PhCO <sub>2</sub> <sup>-</sup> [a]	-6.26	-4.89	-2.10	4.16	298	2.79	444
9	<i>Z-1b</i> ⊃PhCO <sub>2</sub> <sup>-</sup> [b]	-6.44	-4.99	-2.02	4.42	280	2.97	418

[a] anion bound exclusively by one urea group; [b] anion bound by both urea group.



## 2.5 Visualization of the DFT calculated structures

The location of  $\pi$ ,  $n$ , and  $\pi^*$  orbitals, for both *E* and *Z* isomers, were supported by the mapping of the corresponding molecular orbital (MO) onto molecule electronic density ( $\rho = 0.001$  au). However, in several cases the exact position of the  $n$  MO of the corresponding *Z*-isomer could not be unambiguously distinguished due to mixing with other basic orbital from phenylurea and/or benzoate moieties.

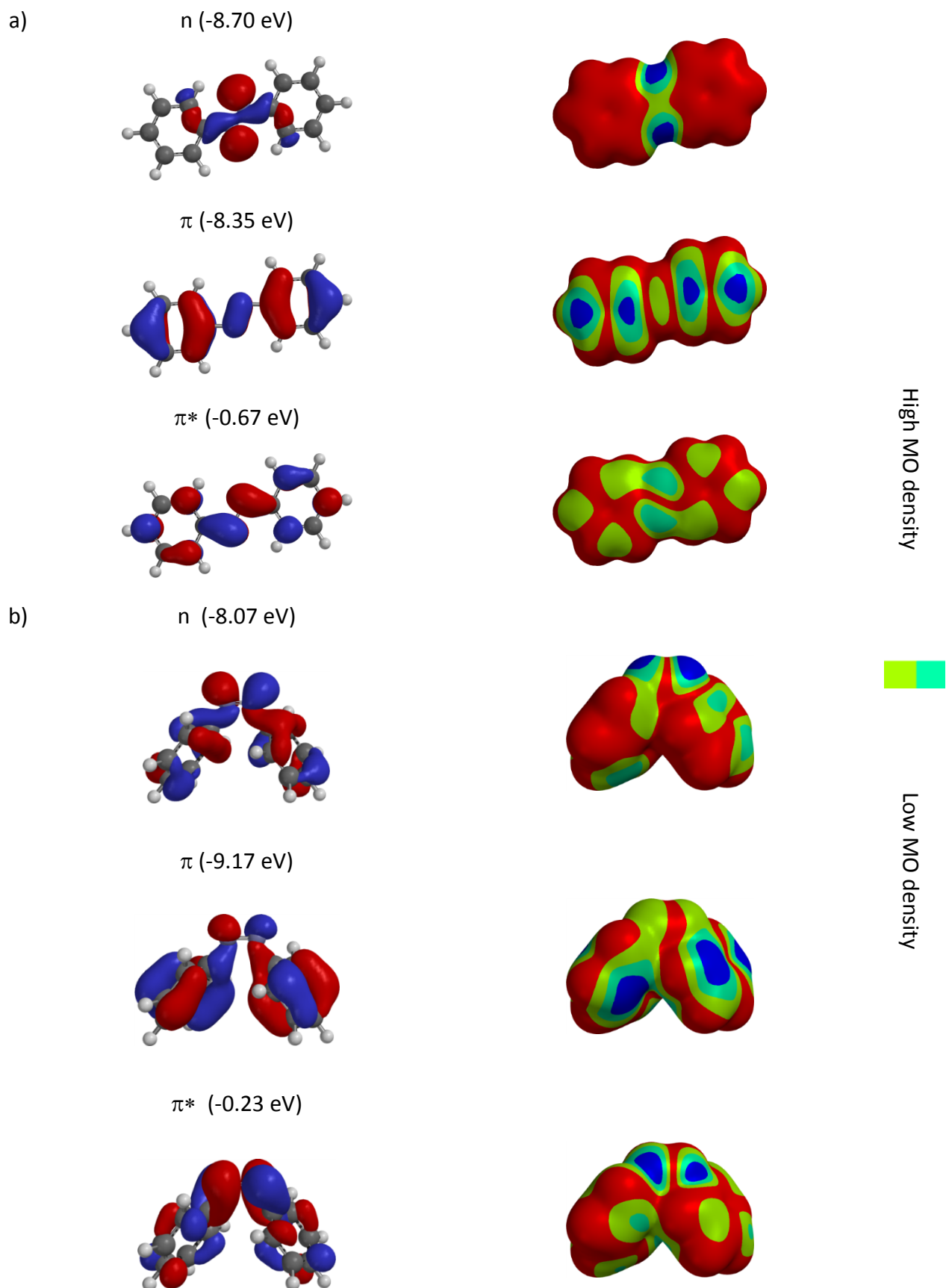


**Fig. S16** Representation of the HOMOs ( $n$ ,  $\pi$ ) and LUMO ( $\pi^*$ ) orbitals of the *E*- (a) and *Z*-isomer (b) of the parent AB calculated at the DFT/ $\omega$ b97x-d/6-31+G\* level of theory, the energy of the corresponding MO is given in parentheses.

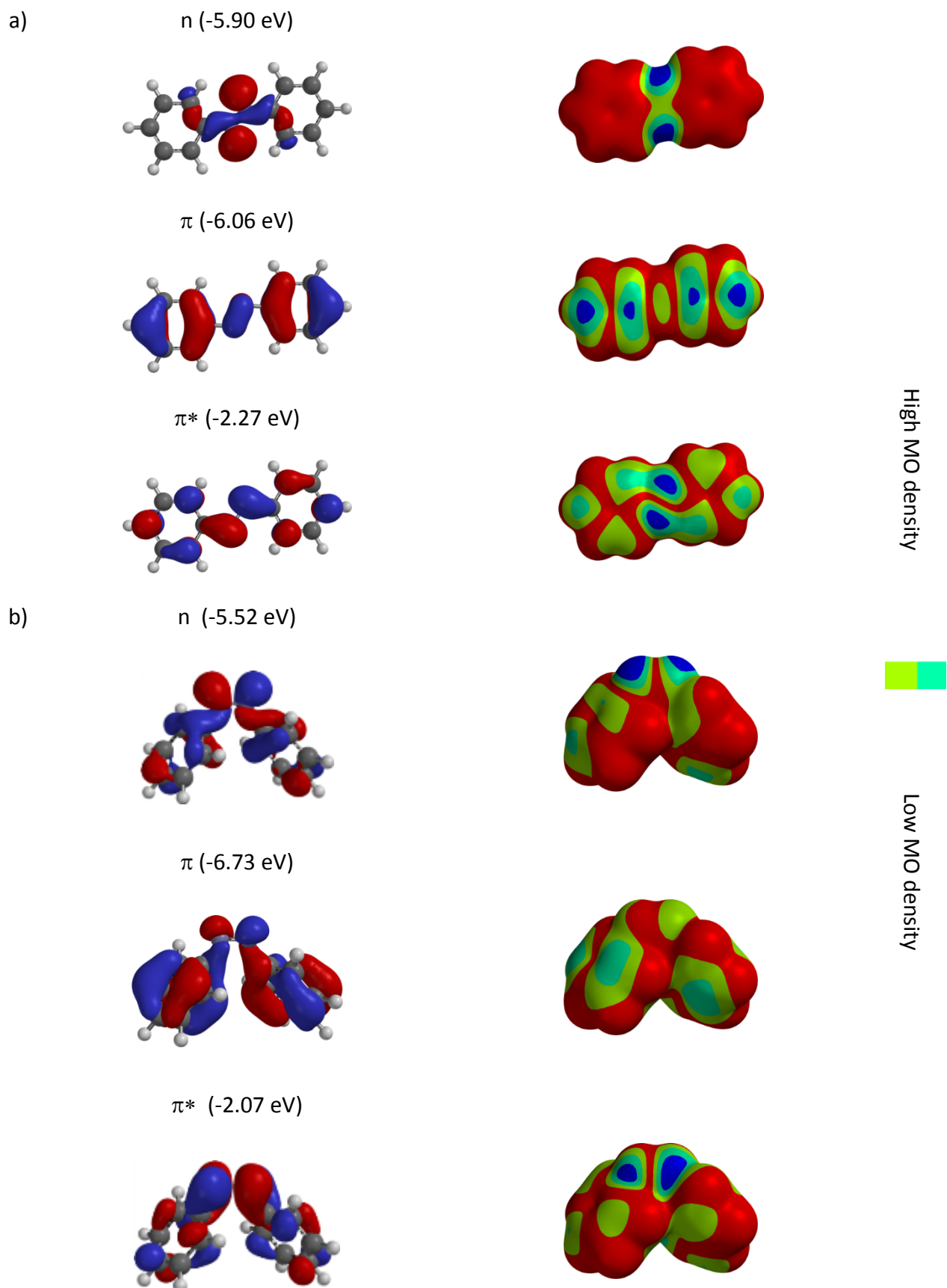


**Fig. S17** Representation of the HOMOs ( $n$ ,  $\pi$ ) and LUMO ( $\pi^*$ ) orbitals of the *E*- (a) and *Z*-isomer (b) of the parent AB calculated at the DFT/EDF2/6-31G\* level of theory, the energy of the corresponding MO is given in parentheses.

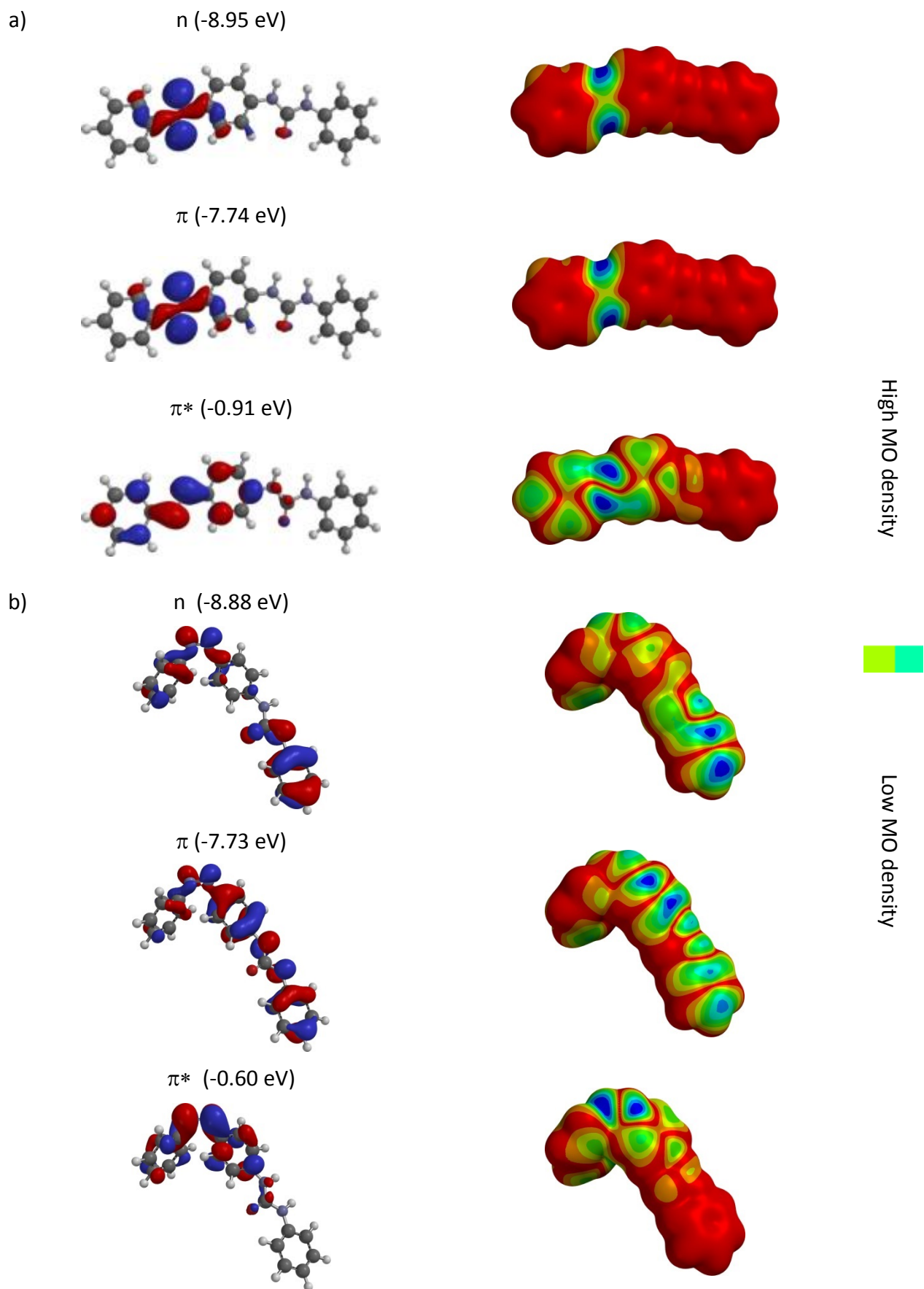


**Fig. S18** Representation of the HOMOs ( $n$ ,  $\pi$ ) and LUMO ( $\pi^*$ ) orbitals of the *E*- (a) and *Z*-isomer (b) of the host **1a** calculated at the DFT/ $\omega$ b97x-d/6-31+G\*/SM8-DMSO level of theory, the energy of the corresponding MO is given in parentheses.

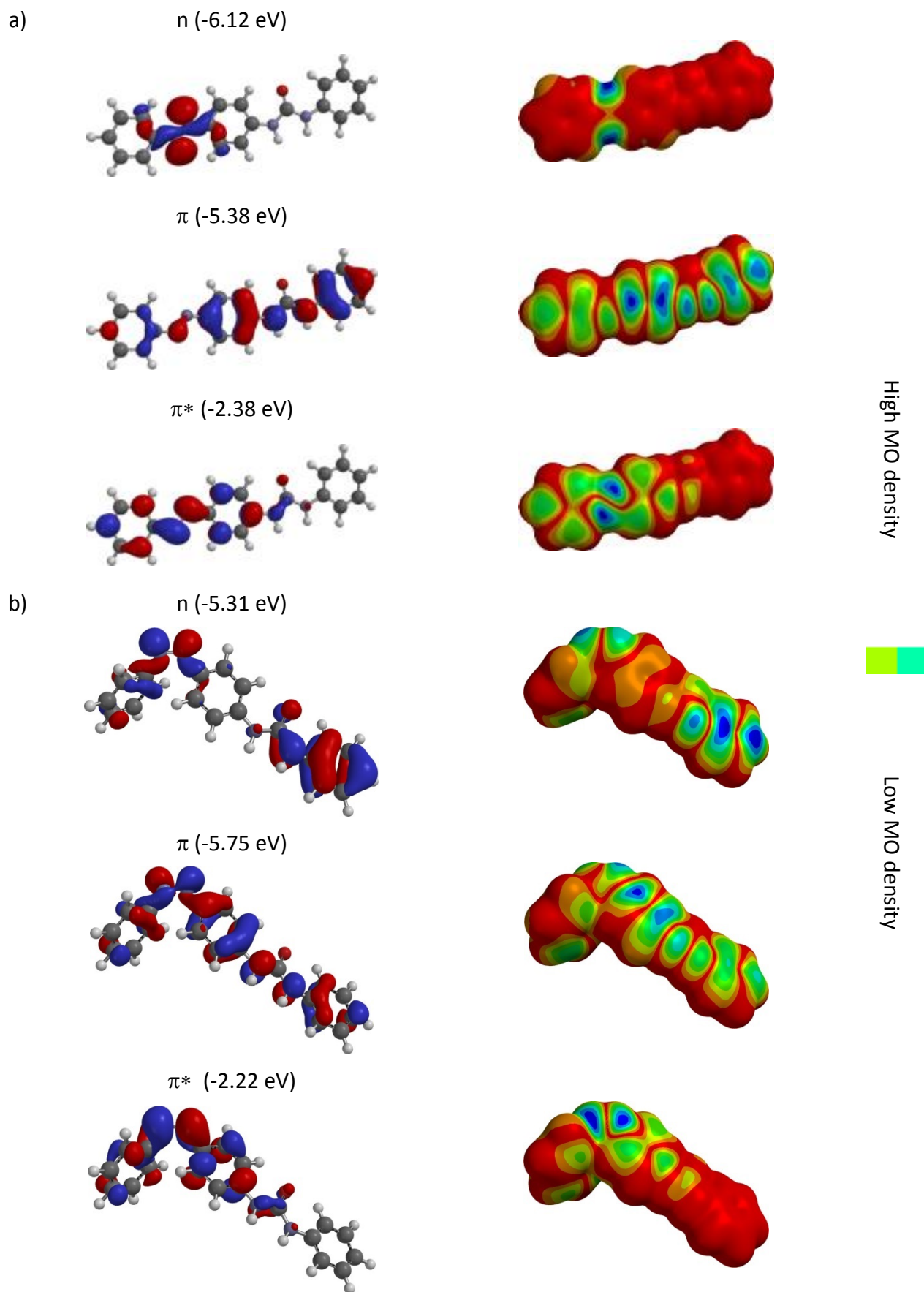


**Fig. S19** Representation of the HOMOs ( $n$ ,  $\pi$ ) and LUMO ( $\pi^*$ ) orbitals of the *E*- (a) and *Z*-isomer (b) of the host **1a** calculated at the DFT/EDF2/6-31G\*/SM8-DMSO level of theory, the energy of the corresponding MO is given in parentheses.

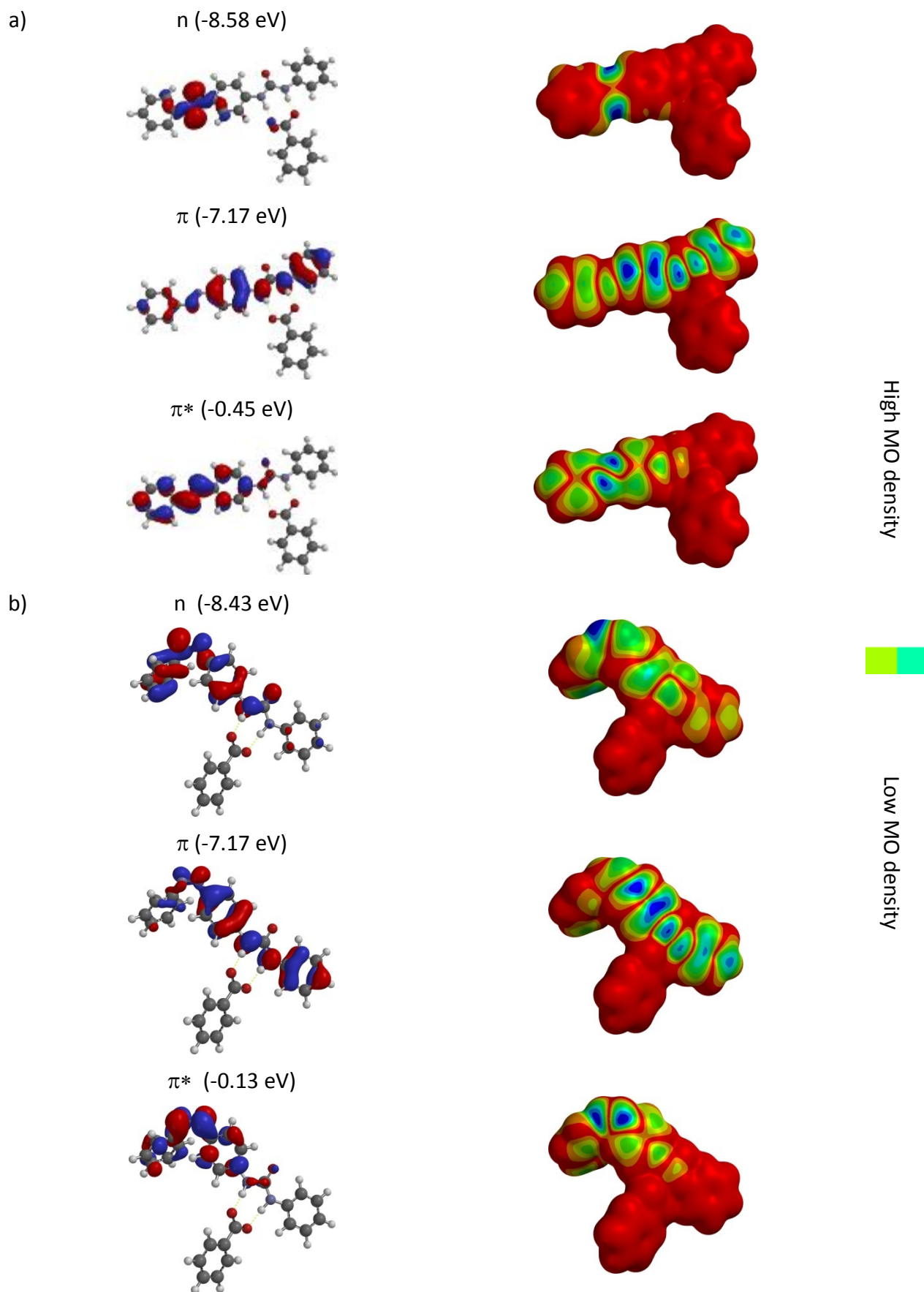


**Fig. S20** Representation of the HOMOs ( $n$ ,  $\pi$ ) and LUMO ( $\pi^*$ ) orbitals of the *E*- (a) and *Z*-isomer (b) of the benzoate complex of the host **1a** calculated at the DFT/ $\omega$ b97x-d/6-31+G\*/SM8-DMSO level of theory, the energy of the corresponding MO is given in parentheses.

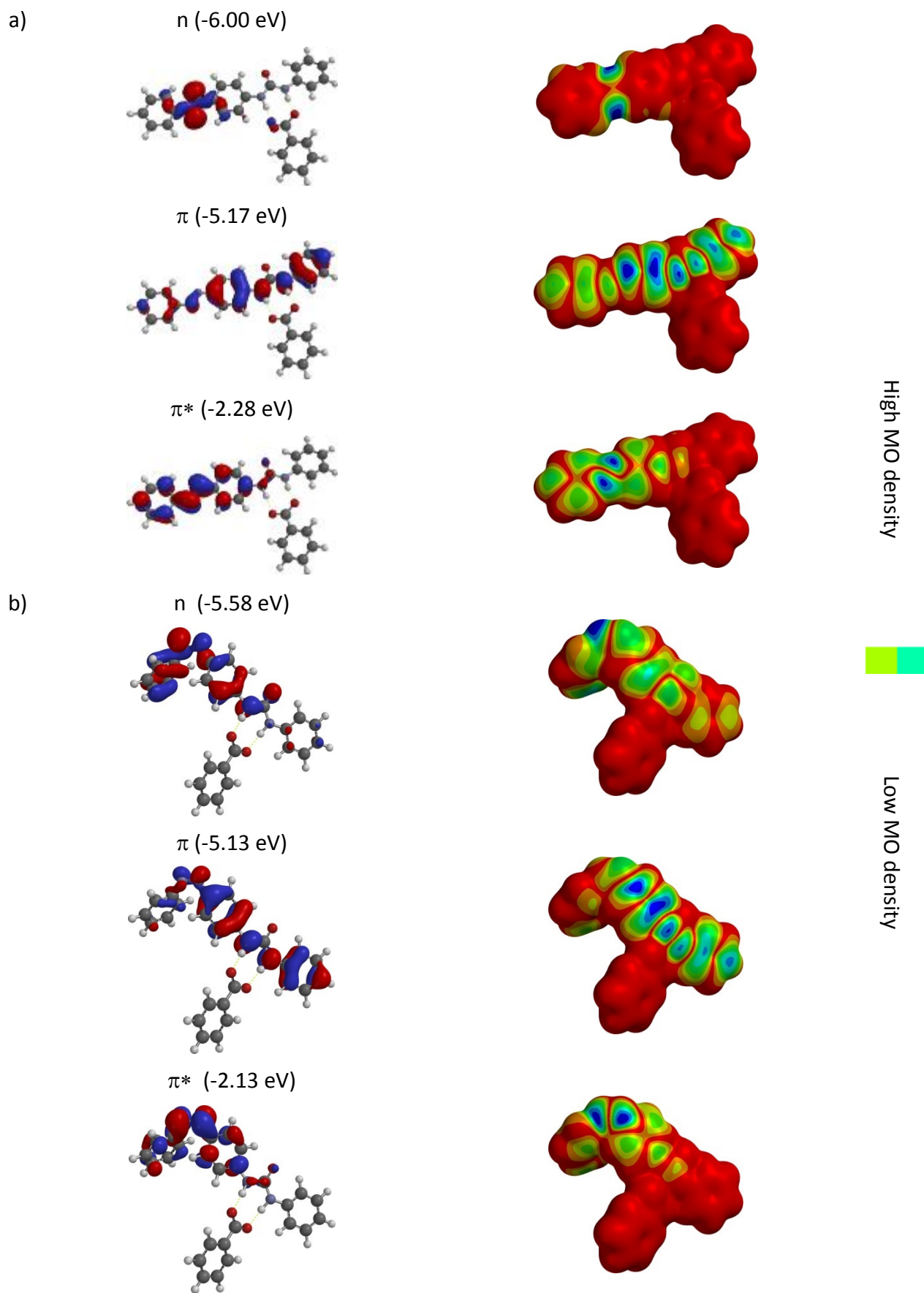


**Fig. S21** Representation of the HOMOs ( $n$ ,  $\pi$ ) and LUMO ( $\pi^*$ ) orbitals of the *E*- (a) and *Z*-isomer (b) of the benzoate complex of the host **1a** calculated at the DFT/EDF2/6-31G\*/SM8-DMSO level of theory, the energy of the corresponding MO is given in parentheses.

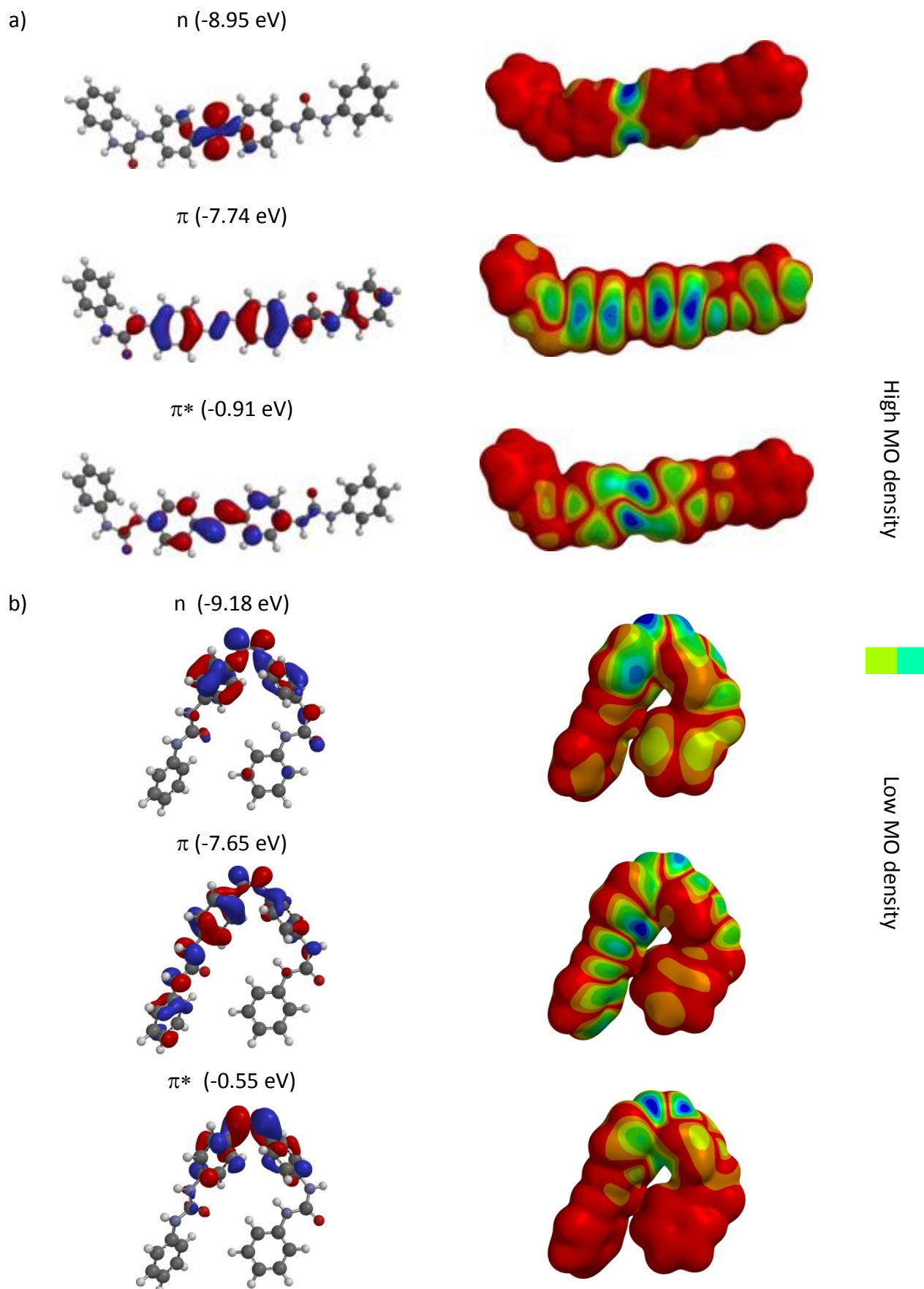


**Fig. S22** Representation of the HOMOs ( $n$ ,  $\pi$ ) and LUMO ( $\pi^*$ ) orbitals of the *E*- (a) and *Z*-isomer (b) of the host **1b** calculated at the DFT/ $\omega$ b97x-d/6-31+G\*/SM8-DMSO level of theory, the energy of the corresponding MO is given in parentheses.



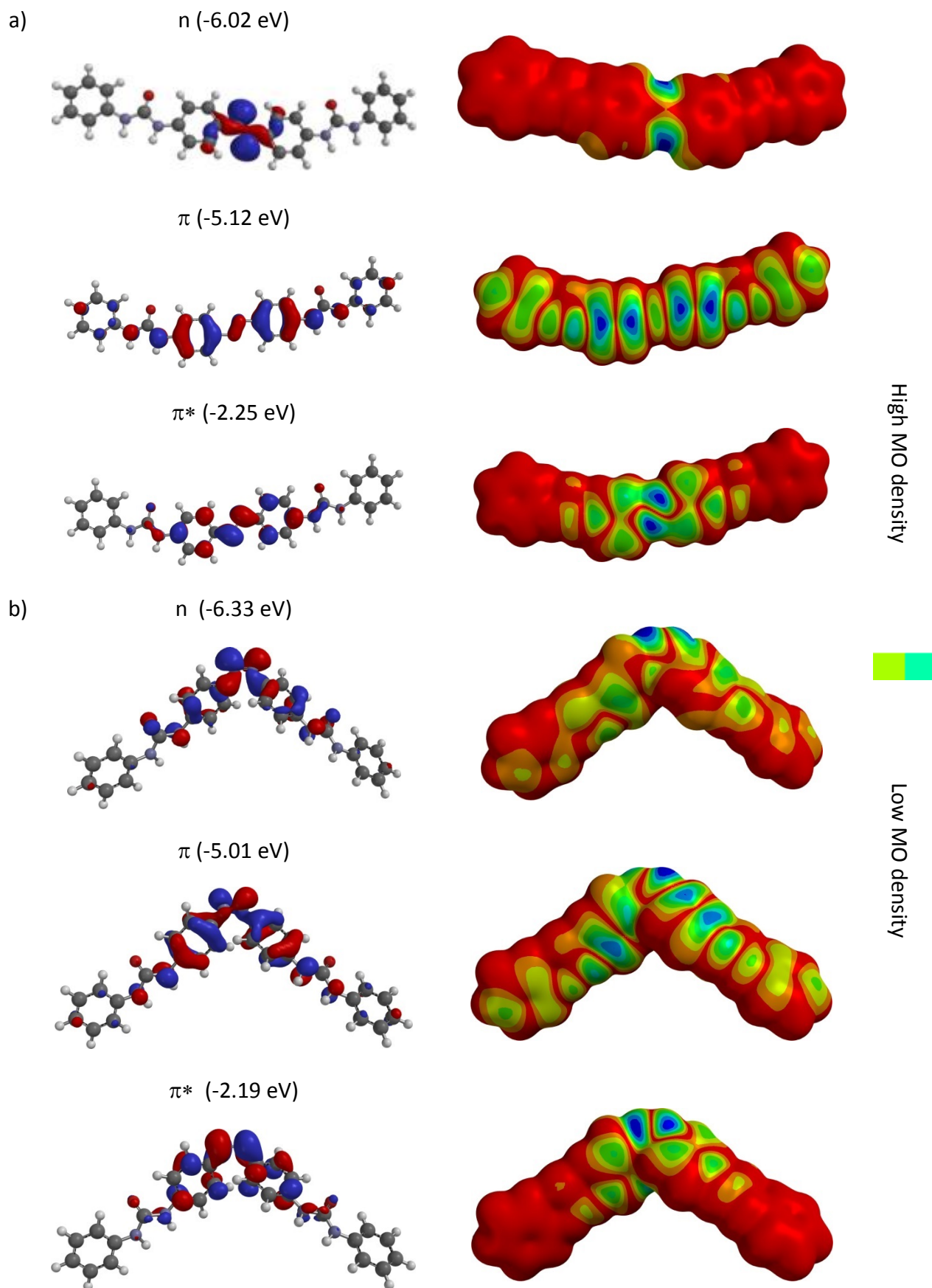


**Fig. S23** Representation of the HOMOs ( $n$ ,  $\pi$ ) and LUMO ( $\pi^*$ ) orbitals of the *E*- (a) and *Z*-isomer (b) of the host **1b** calculated at the DFT/EDF2/6-31G\*/SM8-DMSO level of theory, the energy of the corresponding MO is given in parentheses.

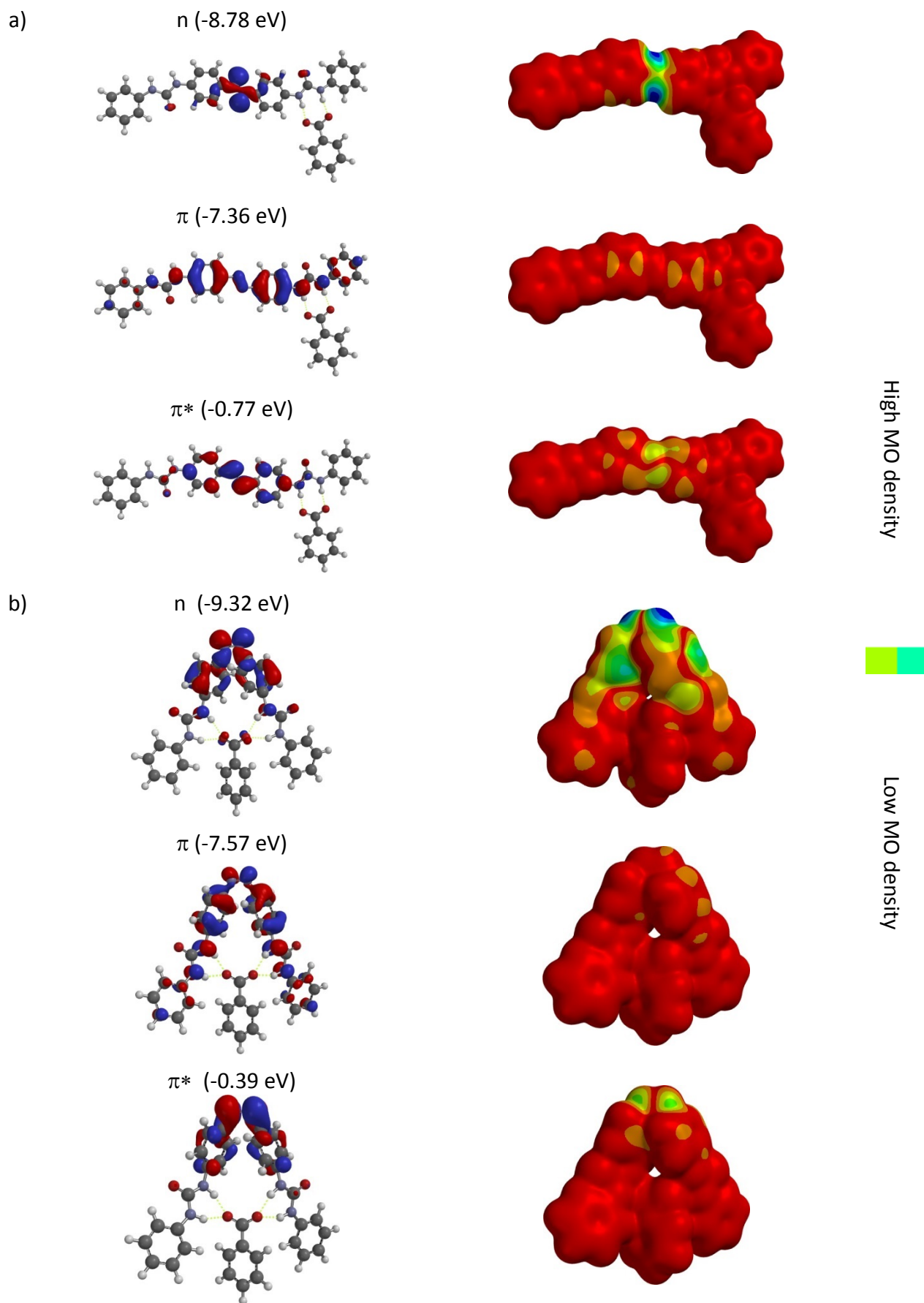


**Fig. S24** Representation of the HOMOs ( $n$ ,  $\pi$ ) and LUMO ( $\pi^*$ ) orbitals of the *E*- (a) and *Z*-isomer (b) of the benzoate complex of the host **1b** calculated at the DFT/ $\omega$ b97x-d/6-31+G\*/SM8-DMSO level of theory, the energy of the corresponding MO is given in parentheses.

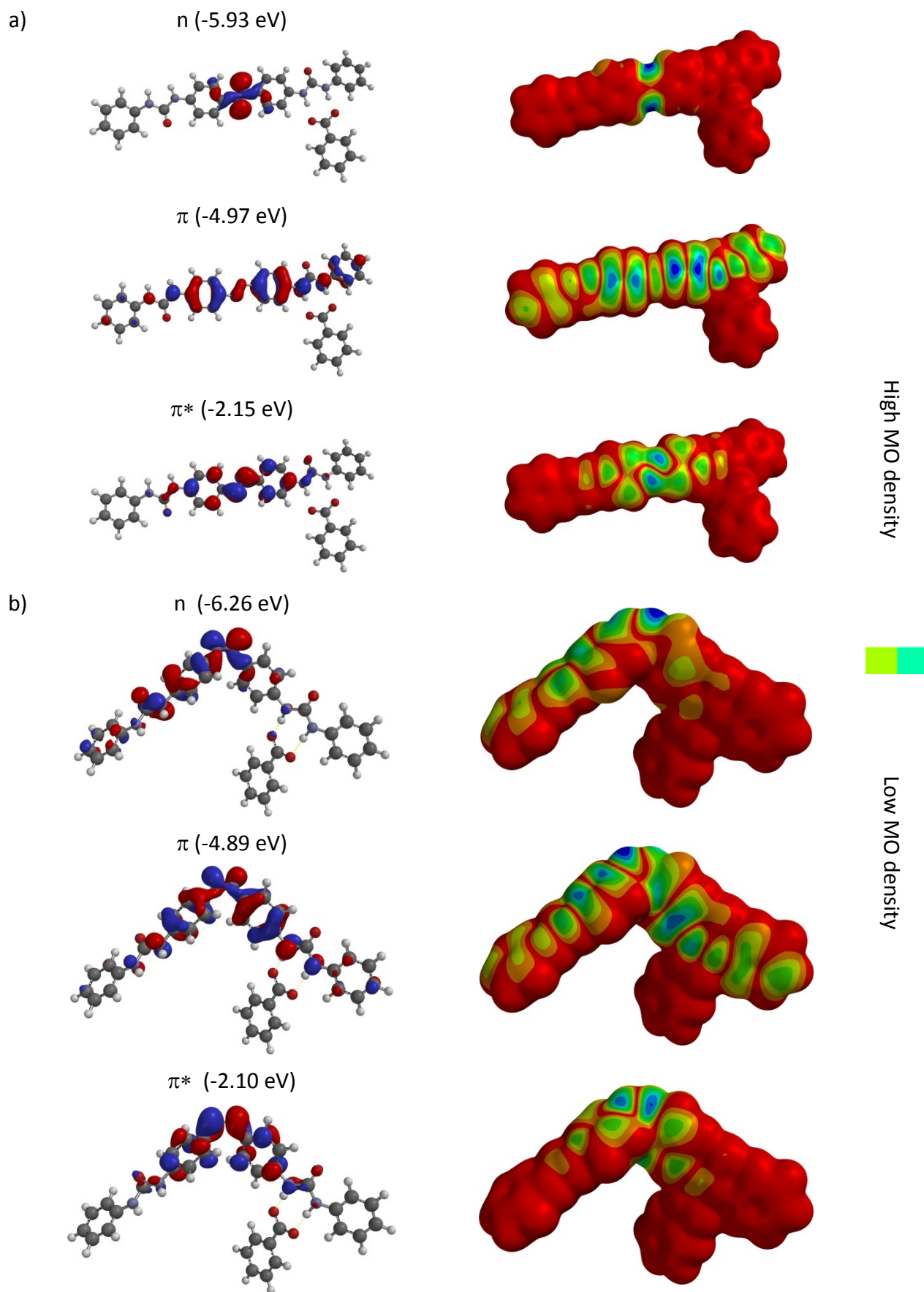


**Fig. S25** Representation of the HOMOs ( $n$ ,  $\pi$ ) and LUMO ( $\pi^*$ ) orbitals of the *E*- (a) and *Z*-isomer (b) of the benzoate complex of the host **1b** calculated at the DFT/EDF2/6-31G\*/SM8-DMSO level of theory, the energy of the corresponding MO is given in parentheses.

## 2.6 Determination of the first-order rate constant $\kappa_{\text{obs}}$ using UV-Vis spectroscopy

The rate of thermal  $Z \rightarrow E$  isomerization of receptors **Z-1** were calculated by monitoring the absorption change of  $Z$  and  $E$  isomers in darkness at  $298.0 \pm 0.1$  K. The observed first-order rate  $\kappa_{\text{obs}}$  is an average of the  $\kappa$  determined by Marquard non-linear technique<sup>24</sup> at four different wavelengths as implemented in Cary WinUV Software 5.0.0.999. In all cases, practically linear Arrhenius and Eyring plots indicate that during  $Z \rightarrow E$  isomerization only one mechanism occurs (Fig. S26 and Tab. S4).

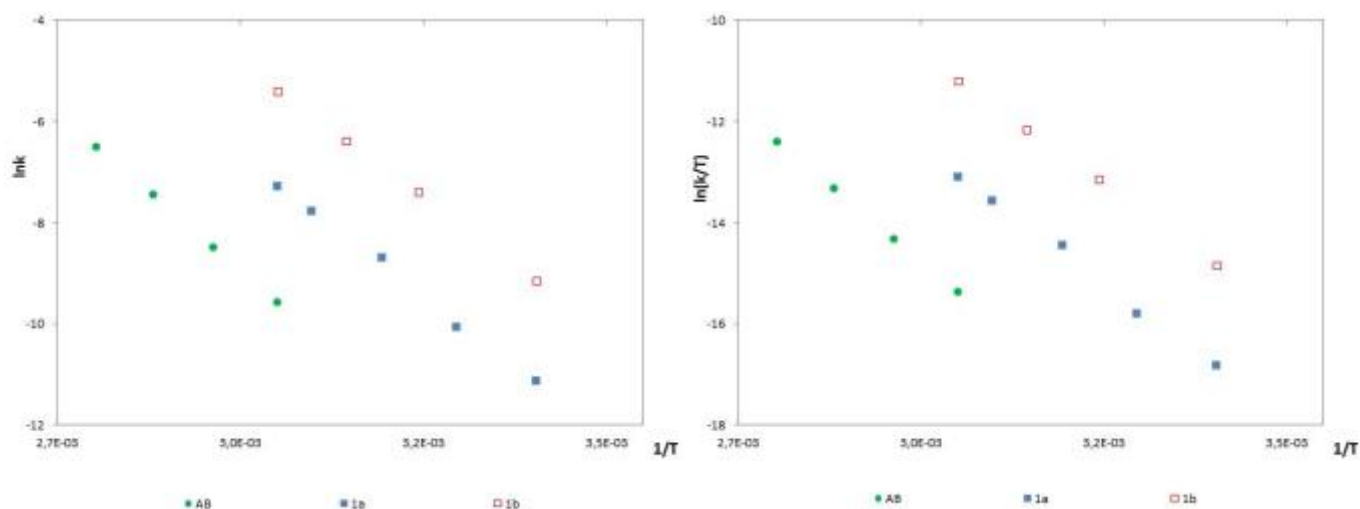


**Fig. S26** Arrhenius (left) and van't Hoff (right) plots of the thermal **Z-1**  $\rightarrow$  **E-1** isomerization.

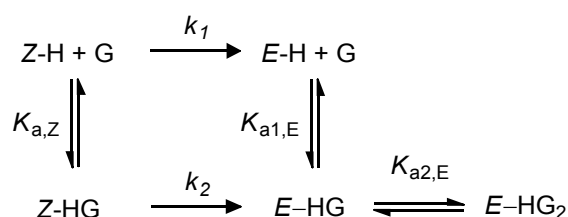
**Tab. S4** Results of the fitting the experimental data for **Z-AB** and **Z-1**<sup>a]</sup>

Host	Guest	Y=Ax+B (Arrhenius plot)			Y=Ax+B (van't Hoff plot)			$\Delta E_a$	$\Delta H^\ddagger$	$T\Delta S^\ddagger$	$\Delta G^\ddagger$
		A	B	R <sup>2</sup>	A	B	R <sup>2</sup>				
AB	none	-12342.17 $\pm$ 58.59	27.48 $\pm$ 0.17	1.000	-11994.53 $\pm$ 60.19	20.63 $\pm$ 0.17	1.000	103	100	-7.8	107
<b>1a</b>	none	-11062.84 $\pm$ 25.95	366.16 $\pm$ 1.16	0.997	-10747.71 $\pm$ 19.19	366.62 $\pm$ 1.16	0.997	92.0 $\pm$ 3.0	89.4 $\pm$ 3.0	-11.3 $\pm$ 0.7	100.7 $\pm$ 3.7
<b>1b</b>	none	-10632.96 $\pm$ 26.53	117.80 $\pm$ 0.37	1.000	-10318.42 $\pm$ 19.78	120.90 $\pm$ 0.38	1.000	88.4 $\pm$ 1.0	85.8 $\pm$ 1.0	-9.9 $\pm$ 0.2	95.7 $\pm$ 1.2

[a] values for  $E_a$ ,  $\Delta H^\ddagger$ ,  $T\Delta S^\ddagger$ , and  $\Delta G^\ddagger$  are given in  $\text{kJ}\cdot\text{mol}^{-1}$ .

## 2.7 Procedure for the determination of association constant $K_{a,Z}$ and first-order rate constant $k_2$ from “ $Z \rightarrow E$ thermal titration” experiment

Assuming that receptor having two binding pockets is able to bind two anions in one form ( $E\text{-H}$ ) and one anion in another form ( $Z\text{-H}$ ), and additionally that anion influences the irreversible transformation of  $Z\text{-H}$  into  $E\text{-H}$ , we can describe the solution equilibria as shown in Scheme S2.



**Scheme S2.** Equilibria describing anion complexation and  $Z \rightarrow E$  isomerisation, H – host, G – guest.

We can express above relations using kinetic and thermodynamic eqn S1-5:

$$\frac{d([Z - HG])}{dt} = -k_2[Z - HG] \quad (S1)$$

$$\frac{d([Z - H])}{dt} = -k_1[Z - H] \quad (S2)$$

$$K_{a,Z} = \frac{[Z - HG]}{[Z - H][G]} \quad (S3)$$

$$K_{a,E} = \frac{[E - HG]}{[E - H][G]} \quad (S4)$$

$$K_{a2,E} = \frac{[E - HG_2]}{[E - HG][G]} \quad (S5)$$

Concentration of Z-H does not depend on the concentration of E-H and so equilibria described by eqn (S4) and eqn (S5) are irrelevant for the Z→E transformation. Therefore one can conclude that the observed kinetic rate constant describing Z→E isomerisation depends on three parameters, namely the association constant of the Z- isomer with guest ( $K_{a,Z}$ ) and two first-order rate constants for free Z-H ( $k_1$ ) and its saturated complex with the corresponding guest ( $k_2$ ). When the total concentration of the guest is much larger than the concentration of the host ( $[G]_0 \gg [H]$ ), which is generally true for UV-Vis titration experiments, one can assume that  $[G] \cong [G]_0$ . Then, after inserting concentration of the HG complex from eqn (S3) to the eqn (S1) and adding eqn (S1) to the eqn (S2), we arrive at eqn (S6) which after simple rearrangements gave eqn (S7) and eqn (S8):

$$\frac{d([Z - HG])}{dt} \left( 1 + \frac{1}{K_{a,Z}[G]_0} \right) = -[Z - HG] \left( k_2 + \frac{k_1}{K_{a,Z}[G]_0} \right) \quad (S6)$$

$$\frac{d([Z - HG])}{dt} = -[Z - HG] \left( \frac{k_1 + k_2 K_{a,Z}[G]_0}{1 + K_{a,Z}[G]_0} \right) = -[Z - HG] \kappa_{obs.} \quad (S7)$$

$$\kappa_{obs.} \equiv f_H k_1 + f_{HG} k_2 = \frac{k_1(1 + k_{enh.} K_{a,Z}[G]_0)}{1 + K_{a,Z}[G]_0} \quad (S8)$$

Constant  $\kappa_{obs.}$  depends only on initial guest concentration ( $[G]_0$ ) and is determined by fitting of the experimental data to the first-order kinetics using the Marquard non-linear technique. Therefore, parameters of interest ( $K_{a,Z}$  and  $k_2$ ) could be determined using a nonlinear regression technique with experimentally determined rate constants ( $\kappa_{obs.}$ ) for various amounts of guest added. During fitting we have noticed that in case when the absolute value of  $k_2$  is very small (in comparison to other variables in eqn (S6) and eqn (S7)), it is better to use the enhancement of the rate constant  $k_{enh.}$  ( $k_2/k_1$ ) for achieving good fit with the experimental data (eqn (S8)). Finally, eqn (S7) after rearrangement of variables followed by integration could be transformed into eqn (S9) which express the concentration of Z-H at any time of the experiment.

$$[Z - HG]_t = [Z - HG]_0 e^{-\kappa_{obs.} t} \quad (S9)$$

Experimental data and results of fitting for the “Z→E thermal titration” of the mixture of EZ-1 with TBA-benzoate are given in Tables S5 and S6, respectively.

**Tab. S5** Experimental data for titration of the Z-1 with TBA-benzoate at 298.0±0.1 K

Exp. no.	Z-1a		Z-1b	
	[G] <sub>0</sub>	$\kappa_{obs.}$	[G] <sub>0</sub>	$\kappa_{obs.}$
1	0,000E+00	1,467E-05	0,000E+00	1,314E-04
2	2,495E-04	2,466E-04	2,499E-04	2,255E-04
3	4,980E-04	3,862E-04	4,997E-04	3,018E-04
4	7,454E-04	4,786E-04	7,494E-04	3,747E-04

5	9,919E-04	5,367E-04	1,248E-03	4,915E-04
6	1,237E-03	6,051E-04	1,747E-03	5,838E-04
7	1,725E-03	6,957E-04	2,742E-03	7,275E-04
8	1,968E-03	6,868E-04	3,736E-03	8,360E-04
9	-	-	4,727E-03	9,250E-04
10	-	-	6,211E-03	1,020E-03
11	-	-	7,690E-03	1,093E-03
12	-	-	9,655E-03	1,170E-03
13	-	-	1,161E-02	1,221E-03
14	-	-	1,405E-02	1,273E-03
15	-	-	1,647E-02	1,322E-03
16	-	-	1,936E-02	1,368E-03
17	-	-	2,224E-02	1,383E-03
18	-	-	2,699E-02	1,411E-03

**Tab. S6** Results of the fitting the experimental data for titration of the Z-1 with TBA-benzoate

Parameter	Z-1a		Z-1b	
	Value	Error	Value	Error
Chi <sup>2</sup>	1.9533E-10	-	5.5459E-11	-
R <sup>2</sup>	0.9970	-	0.9997	-
K <sub>a,z</sub>	1342.46	97.16	249.53	3.48
k <sub>enh</sub>	64.60	1.69	12.21	0.05
k <sub>1</sub>	1,467E-05	Fixed	1,314E-04	Fixed











C	6.474166	-3.835895	2.115385	C	2.601270	6.031718	0.724106
H	6.433879	-4.911546	2.291766	H	2.993393	6.933762	0.265133
C	5.441914	-3.210247	1.420253	C	3.157397	4.798444	0.406413
H	4.593767	-3.775340	1.047957	H	3.979877	4.711830	-0.294828

## References

1. H. Kuhn, S. Braslavsky and R. Schmidt, *Pure Appl. Chem.*, 2004, **76**, 2105-2146.
2. C. Frassinetti, L. Alderighi, P. Gans, A. Sabatini, A. Vacca and S. Ghelli, *Anal. Bioanal. Chem.*, 2003, **376**, 1041-1052.
3. C. Frassinetti, S. Ghelli, P. Gans, A. Sabatini, M. S. Moruzzi and A. Vacca, *Anal. Biochem.*, 1995, **231**, 374-382.
4. A. J. Lowe, F. M. Pfeffer and P. Thordarson, *Supramol. Chem.*, 2012, **24**, 585-594.
5. P. Thordarson, *Chem. Soc. Rev.*, 2011, **40**, 1305-1323.
6. K. A. Connors, *Binding constants: the measurement of molecular complex stability*, Wiley New York, 1987.
7. P. Job, *Ann. Chim.*, 1928, **9**, 113-203.
8. A. V. Marenich, R. M. Olson, C. P. Kelly, C. J. Cramer and D. G. Truhlar, *J. Chem. Theory Comput.*, 2007, **3**, 2011-2033.
9. Spartan'10 for Windows, **2011**.
10. A. D. Becke, *The Journal of Chemical Physics*, 1993, **98**, 5648-5652.
11. D. Bléger, J. Schwarz, A. M. Brouwer and S. Hecht, *J. Am. Chem. Soc.*, 2012, **134**, 20597-20600.
12. J.-D. Chai and M. Head-Gordon, *J. Chem. Phys.*, 2009, **131**, -.
13. J.-D. Chai and M. Head-Gordon, *Phys. Chem. Chem. Phys.*, 2008, **10**, 6615-6620.
14. All calculations were performed using Spartan'10 for Windows (Wavefunction Inc., California, USA, 2011)
15. J. M. Smith, Y. Jami Alahmadi and C. N. Rowley, *J. Chem. Theory Comput.*, 2013, **9**, 4860-4865.
16. G. Bravo-Pérez and H. Saint-Martin, *Int. J. Quantum Chem.*, 2012, **112**, 3655-3660.
17. O. A. Vydrov and T. Van Voorhis, *J. Chem. Theory Comput.*, 2012, **8**, 1929-1934.
18. S. Grimme, *Wiley Interdisciplinary Reviews: Computational Molecular Science*, 2011, **1**, 211-228.
19. L. Goerigk and S. Grimme, *Phys. Chem. Chem. Phys.*, 2011, **13**, 6670-6688.
20. J.-D. Chai and M. Head-Gordon, *Chem. Phys. Lett.*, 2008, **467**, 176-178.
21. J. A. Bouwstra, A. Schouten and J. Kroon, *Acta Crystallographica Section C*, 1983, **39**, 1121-1123.
22. D. Armstrong, J. Clarkson and W. Smith, *The Journal of Physical Chemistry*, 1995, **99**, 17825-17831.
23. A. Mostad and C. Rømming, *Acta Chem. Scand*, 1971, **25**, 3561-3568.
24. L. M. Schwartz and R. I. Gelb, *Anal. Chem.*, 1978, **50**, 1592-1594.